COPPE
Instituto Alberto Luiz Coimbra de Pós-Graduação e Pesquisa de Engenharia
UFRJ

DETERMINATION OF THE TRANSVERSE DISPERSION COEFFICIENT IN PORE NETWORKS USING THE SUB-VOLUME ANALYSIS

Matheus Rocha Marques de Almeida

Dissertação de Mestrado apresentada ao Programa de Pós-graduação em Engenharia Química, COPPE, da Universidade Federal do Rio de Janeiro, como parte dos requisitos necessários à obtenção do título de Mestre em Engenharia Química.

Orientadores: Paulo Laranjeira da Cunha Lage
Paulo Couto

Rio de Janeiro
Fevereiro de 2024

DETERMINATION OF THE TRANSVERSE DISPERSION COEFFICIENT IN PORE NETWORKS USING THE SUB-VOLUME ANALYSIS

Matheus Rocha Marques de Almeida

DISSERTAÇÃO SUBMETIDA AO CORPO DOCENTE DO INSTITUTO ALBERTO LUIZ COIMBRA DE PÓS-GRADUAÇÃO E PESQUISA DE ENGENHARIA DA UNIVERSIDADE FEDERAL DO RIO DE JANEIRO COMO PARTE DOS REQUISITOS NECESSÁRIOS PARA A OBTENÇÃO DO GRAU DE MESTRE EM CIÊNCIAS EM ENGENHARIA QUÍMICA.

Orientadores: Paulo Laranjeira da Cunha Lage
Paulo Couto

Aprovada por: Prof. Paulo Laranjeira da Cunha Lage
Prof. Paulo Couto
Prof. Gabriel Gonçalves da Silva Ferreira
Prof. Celso Peres Fernandes

RIO DE JANEIRO, RJ – BRASIL
FEVEREIRO DE 2024

Rocha Marques de Almeida, Matheus

Determination of the transverse dispersion coefficient in pore networks using the sub-volume analysis/Matheus Rocha Marques de Almeida. – Rio de Janeiro: UFRJ/COPPE, 2024.

XX, 67 p.: il.; 29, 7cm.

Orientadores: Paulo Laranjeira da Cunha Lage

Paulo Couto

Dissertação (mestrado) – UFRJ/COPPE/Programa de Engenharia Química, 2024.

Referências Bibliográficas: p. 55 – 62.

1. Pore network. 2. Transverse dispersion coefficient. 3. OpenPNM. I. Laranjeira da Cunha Lage, Paulo *et al.* II. Universidade Federal do Rio de Janeiro, COPPE, Programa de Engenharia Química. III. Título.

"A ciência serve para nos dar uma ideia de quão extensa é a nossa ignorância."

Félicité Robert de Lamennais

Agradecimentos

Gostaria de agradecer primeiramente a Deus por sua imensa misericórdia e favor em minha vida e por todos os benefícios que tenho vivido por Seu amor. Agradeço a minha esposa, Júlia Moraes da Costa Marques, por sempre estar ao meu lado durante todos os momentos. Seu carinho, amor e cumplicidade tiveram papéis fundamentais durante essa minha trajetória. Igualmente agradeço ao meu pai (*in memoriam*), Milton Marques, que sempre foi um grande espelho para mim como pessoa, pai e profissional. Minha mãe, Vitalina Marques, e irmão, Filipe Marques, por serem tão presentes na minha vida. Agradeço também imensamente aos meus amigos de laboratório, Alex Machado, Lauren Schlatter, Manoela Mariotini e César Timaná pela amizade, companherismo e momentos divertidos e icônicos que vivemos juntos. Por último, mas não menos importante, minha gratidão aos professores Paulo Lage e Paulo Couto pelo apoio durante toda a trajetória acadêmica que vivi durante esse período de mestrado. Seus conselhos foram muito valiosos para mim e os guardarei para toda uma vida.

Resumo da Dissertação apresentada à COPPE/UFRJ como parte dos requisitos necessários para a obtenção do grau de Mestre em Ciências (M.Sc.)

DETERMINAÇÃO DO COEFICIENTE DE DISPERSÃO TRANSVERSAL EM REDE DE POROS UTILIZANDO ANÁLISE DE SUB-VOLUMES

Matheus Rocha Marques de Almeida

Fevereiro/2024

Orientadores: Paulo Laranjeira da Cunha Lage
Paulo Couto

Programa: Engenharia Química

O presente trabalho tem o objetivo de desenvolver uma metodologia para determinação do coeficiente de dispersão transversal de resultados de simulação do transporte de massa de rede de poros de diferentes tipos, onde o *software* OpenPNM-v2.6.0® foi utilizado. Para isto, dados de concentração e seus desvios-padrões são extraídos das simulações e comparadas com a solução analítica desenvolvida para determinação da razão entre o coeficiente de dispersão longitudinal e o de dispersão transversal. Uma vez conhecido o primeiro e seu erro a 95% de confiança, pode-se determinar segundo com o seu respectivo erro. As dimensões e o número de realizações da rede de poros, bem como o seu número Péclet microscópico foram fatores avaliados. Dessa forma, mostrou-se que o valor do coeficiente de dispersão transversal é praticamente igual para o mesmo tipo de rede e para o mesmo valor de número de Péclet microscópico, não dependendo do comprimento da rede, desde que o completo desenvolvimento da camada limite de concentração seja alcançado. Mudanças na largura do domínio não diminuíram significativamente o erro de determinação da razão dos coeficientes de dispersão. Entretanto, mostrou-se que o coeficiente de

dispersão transversal é sensível à largura da rede de poros. Além disso, o uso de diferentes realizações da rede de poros tem pouca influência no valor determinado para tal coeficiente.

Abstract of Dissertation presented to COPPE/UFRJ as a partial fulfillment of the requirements for the degree of Master of Science (M.Sc.)

DETERMINATION OF THE TRANSVERSE DISPERSION COEFFICIENT IN PORE NETWORKS USING THE SUB-VOLUME ANALYSIS

Matheus Rocha Marques de Almeida

February/2024

Advisors: Paulo Laranjeira da Cunha Lage

Paulo Couto

Department: Chemical Engineering

The present work aims to develop a methodology to determine the transverse dispersion coefficient from performed simulation of mass transport in different types of pore networks, where the *software* OpenPNM-v2.6.0® was used. Concentration data and their standard deviations are extracted from these simulations and compared with the developed analytical solution to determine the ratio between the longitudinal and transverse dispersion coefficients. Once the former and its 95% confidence error are known, the latter and its error can be determined. The dimensions and the number of realisations of the pore networks and the microscopic Péclet number were evaluated. In this way, it is shown that the transverse dispersion coefficient value is almost equal for the same type of network and the value of the microscopic Péclet number once the complete development of the concentration boundary layer is achieved. Changes in the domain width did not significantly reduce the error of the ratio between both coefficients. However, it is shown that the transverse dispersion coefficient is sensitive to the width of the pore network. Moreover, using different realisations of the pore networks has little influence on the determination of such coefficient.

Contents

List of Figures

List of Tables

List of Symbols

A	Ratio between the length of the domain and its half height
B	Half height of the pore network domain
C	Mean concentration per unit of fluid volume
C_{in}	Solute concentration in the inlet
C_w	Solute concentration in the top and bottom walls of the domain
c	Concentration at pore scale
c_p	Volume-averaged solute concentration
D	Diameter of the column
D_a	Apparent longitudinal diffusivity
$\mathbf{D}$	Dispersion tensor
D_L	Longitudinal dispersion coefficient
D_m	Molecular diffusion coefficient
D_T	Transverse dispersion coefficient
$\mathcal{D}_v$	Dimensionless longitudinal dispersion coefficient
$\mathcal{D}_{vt}$	Dimensionless transverse dispersion coefficient

d	Particle diameter
d_τ	Nominal diameter of Rasching rings
d_i	Diameter of the pore i
d_j	Diameter of the pore j
d_{ij}	Diameter of throat connecting pore i to j
d_p	The equivalent-sphere-volume diameter of the packing material
E	Eddy diffusivity
e_{95}	95% confidence error
$\hat{\mathbf{e}}_x$	Cartesian coordinate system unit vectors in x direction
G	Mass flow rate
g_i^h	Hydraulic conductance of pore i
$g_{c,ij}^h$	Mass transfer conductance of the conduit between pores i and j
g_j^h	Hydraulic conductance of pores j
g_{ij}^h	Hydraulic conductance of the throat connecting pore i to j
K_x	Permeability in x direction
L	Length of the domain
$\mathcal{L}$	Dimensionless sub-volume thickness
L_x	Length of the domain in x direction
L_y	Length of the domain in y direction
L_z	Length of the domain in z direction
l_{ij}	Length of throat connecting pore i to j

l_{pp}	Pore-to-pore distance
l_v	Sub-volume thickness
$\dot{m}_{ij}$	Net flux of diffusion and advection from pore i to pore j
N_{Layer}	Index of the pore layer in to flow direction
N_p	Total number of pores
N_ζ	Number of points within ζ interval
n_p	Total number of pores in the sub-volume
P	Pressure
Pe_L	Longitudinal Péclet number
Pe_B	Transverse Péclet number
Pe_m	Microscopic Péclet number
p_i	Pressure in pore i
p_j	Pressure in pore j
Q	Total volumetric flow rate
q_{ij}	Flow rate from pore i to j
R	Ratio between the longitudinal and transverse dispersion coefficient
r_{1n}	Positive root in the macroscopic model solution
r_{2n}	Negative root in the macroscopic model solution
Re	Reynolds number
T	Dimensionless time
t	Time

$\bar{u}$	Average (intergranular) velocity
$\mathbf{U}$	The fluid velocity vector in porous space
$\mathbf{u}$	Superficial velocity vector
V_i	Volume of pore i
$\mathbf{v}$	Mean intrinsic velocity vector
v_x	Interstitial velocity in x direction
x	Longitudinal direction, parallel to mean flow
x_p	Barycenter position
$x_{p,i}$	Barycenter position of pore i
y	Direction orthogonal to the mean flow
Z_i	Coordination number of pore i

Greek Letters

Δ	Difference between the final and initial value
ε	porosity
η	Dimensionless transversal coordinate to the flow
λ_n	Eigenvalue
μ	Viscosity of the fluid
ν	Kinematic viscosity
ϕ	Dimensionless concentration
δ	Standard deviation
ζ	Dimensionless parallel coordinate to the flow

Mathematical Operations

$\overline{()}^a$	Arithmetic mean
$\bar{\phi}(\zeta_i)$	Mean value of dimensionless concentration in each ζ position

Subscripts

$2h$	Network with its height duplicated from the original
f	Final value
max	Maximum value
min	Minimum value
V	Volumetric

Superscript

$+$	Parameter increased by its 95% confidence error
-	Parameter decreased by its 95% confidence error
eff	Effective
k	Sub-volume index

Abbreviations

ADM	Advection-dispersion model
DNS	Direct Numerical Simulation
FVM	Finite Volume Method
LBM	Lattice Boltzmann method
MCM	Mixed Cell Method
NMR	Nuclear Magnetic Resonance

ODR	Orthogonal Distance Regression
PCG	Permuted Congruential Generator
PDE	Partial Differential Equation
PNM	Pore Network Models
REV	Representative Elementary Volume
SPH	Smoothed Particle Hydrodynamics
SVA	Sub-Volume Analysis
VAM	Volume Averaging Method

Chapter 1

Introduction

In several natural processes and industrial applications, the understanding of solute transport in porous media is crucial, as in contaminant hydrogeology (BEAR, 1988), brain microcirculation (BERG *et al.*, 2020), geological carbon dioxide storage (MEHMANI and XU, 2022b), among others (MEHMANI and XU, 2022a; VAN GORP *et al.*, 2023). It was only in the 1950s that this subject became systematically studied by geophysicists, petroleum and chemical engineers and others. BERG *et al.* (2020) stated that dispersion occurs in the presence of pressure and concentration gradients originating a velocity field in pore scales. This phenomenon can be understood as a contribution of molecular diffusion, advection and mechanical dispersion. Molecular diffusion is due to the random thermal motion of solute molecules or particles, while mechanical dispersion arises from the variability in the flow field. Conversely, advection is related to the transport of molecules or particles by the bulk flow.

Since the first works of SLICHTER (1905), TAYLOR (1953) and ARIS (1956, 1959), many others works attempted to correctly describe the principles of solute dispersion in packed bed of inert particles (BEAR, 1988; DORWEILER and FAHIEN, 1959). BRENNER (1980) formulated a comprehensive theory for determining how particles move through regularly patterned porous materials subjected to fluid flow, indicating that dispersion models remain accurate over extended regions in spatially periodic porous media. CARBONELL and WHITAKER (1983) corroborated this

assertion, asserting its applicability to all porous mediums. GRAY (1975), BEAR (1988) and WHITAKER (1967) elucidated the correct formulation of the transport equation governing the average solute concentration within the porous medium. They accomplished this by employing the volume or spatial averaging method, introduced by SLATTERY (1972).

GRAY (1975), BEAR (1988) and WHITAKER (1967) introduced the volume-average methodology to determine the dispersion coefficient, conducting detailed computational studies for two-dimensional spatially periodic porous media. EIDSATH *et al.* (1983) subsequently applied these spatially periodic models to compute longitudinal and transversal dispersion coefficients in packed beds, comparing their findings with experimental data. However, their longitudinal dispersion coefficient exhibited a stronger dependence on the Péclet number, while the transverse dispersion did not. Soils or underground reservoirs have significant nonuniformities at large scales resulting in dispersion coefficient values that diverge considerably from those observed in packed beds. For these cases, spatially periodic models are inadequate without adjustment to provide accurate results. Alternative approaches have been explored to correlate and forecast dispersion coefficients, adopting a probabilistic framework where the porous medium is geometrically approximated by a pore network composed of cylindrical capillaries characterised by probability distribution functions.

Numerous researchers employing diverse experimental methodologies have extensively investigated dispersion in porous media (BARON, 1952; COELHO and DE CARVALHO, 1988; ROBBINS, 1989). Nevertheless, according to SCHEIDEGGER (1957), longitudinal and transversal dispersion measurements are typically conducted separately, with the consensus that experiments on transversal dispersion are notably more challenging than those focusing on longitudinal dispersion. When a fluid transverses a bed of inert particles, dispersion occurs due to the combined influences of molecular diffusion and advection within the interstitial spaces. Typically, the longitudinal dispersion coefficient is greater than the transversal one

by a factor of 5 for Reynolds numbers exceeding 10. At low Reynolds numbers ($Re < 1$), both dispersion coefficients approximate each other and align with the molecular diffusion coefficient.

The intricate structures of porous media exhibit significant irregularities, whose statistical properties are only partially known. Attaining an exact solution to characterise fluid flow within such structures proves practically unfeasible. Nevertheless, employing the method of volume averaging developed by WHITAKER (1967), the derivation of the transport equation for the average solute concentration in a porous media is formulated.

The quantitative dispersion analysis relies on the generalised Fick's law, incorporating specific dispersion coefficients in the macroscopic scale. Cross-stream dispersion correlates with the transverse dispersion coefficient, D_T, while streamwise dispersion is associated with the longitudinal dispersion coefficient, D_L. Running experiments is time-consuming, especially when different conditions have to be tested. So, numerical experiments take place to supply this necessity to verify other behaviours for distinct scenarios.

Pore-scale modelling is a powerful tool to understand how solute transport occurs in porous media capturing the pore-scale physics. Mainly, two modelling strategies are used: Direct Numerical Simulation (DNS) and Pore Network Modelling (PNM) (BLUNT *et al.*, 2013; GOLPARVAR *et al.*, 2018; YANG *et al.*, 2016). DNS is the methodology where governing equations of flow and transport are solved directly using mathematical methods such as the Finite Volume Method (FVM) (FERRARI and LUNATI, 2014; KOU *et al.*, 2023), Smoothed Particle Hydrodynamics (TARTAKOVSKY *et al.*, 2007) and Lattice Boltzmann Methods (LBM) (XIE *et al.*, 2021). Although DNS yields the highest accuracy and fidelity to the actual behaviour within dispersion in porous media, it is computationally expensive. On the other hand, PNM reduces the complexity of pore structures to network elements, calculating the transport properties of network elements analytically or semi-analytically, allowing for lessening the computational cost, and also giving insight into the over-

all behaviour of solute transport in porous media (LIU *et al.*, 2022; WEISHAUPT *et al.*, 2019).

MACHADO *et al.* (2023) recently proposed a new method called sub-volume analysis (SVA), which uses data from pore network simulations to estimate the longitudinal dispersion coefficient and its associated error. However, this technique has not yet been extended to determine the transverse dispersion coefficient.

1.1 Objectives

The main objective of this work was to employ a sub-volume analysis (SVA) to determine the transverse dispersion coefficient in different types of pore networks at different values for the Péclet number. The simulations were performed using OpenPNM v2.6.0 - an open-source software written in Python. This work also aimed to verify the effect of different network realisations on the value of the transverse dispersion coefficient.

1.2 Document Structure

A literature review is given in Chapter 2, outlining some of the most historically relevant experimental observations to determine transverse and longitudinal dispersion coefficient and their hardship. The methodology is presented in Chapter 3, giving a detailed description of the models used in this work and a conceptual description of the studied cases. The numerical procedure is presented in Chapter 4, with the implementation details, boundary conditions, algorithms and their tolerances used for simulating the flow with solute transport. Results and conclusions are given in Chapters 5 and 6, respectively.

Chapter 2

Literature review

2.1 Longitudinal dispersion

Over the last decades, longitudinal dispersion for flows in porous media has been extensively studied and correlated for both liquid and gaseous systems. A slice of the tremendous amount of published papers on this subject can be found in scientific journals and publications, like the works of CHAO and HOELSCHER (1966), EDWARDS and RICHARDSON (1968), GUNN (1969); LEVENSPIEL and SMITH (1957). The first experimental study aiming at to understanding the longitudinal dispersion dates back to the 1950 (DANCKWERTS, 1953). This study focused on predicting the residence time distribution in continuous contacting packed columns, such as chemical reactors. He provided a new methodology to measure the axial dispersion rates in columns packed with Rasching rings.

Building upon the previous work, KRAMERS and ALBERDA (1953) conducted a theoretical and experimental where they suggested representing packed beds as a sequence of well-mixed regions rather than a sequence of stirred tanks (mixing-cell model) and proposed a $Pe_d(= D_a/\bar{u}d_\tau)$ value close to 1 for Reynolds number ($Re_d = \bar{u}d_\tau/\nu$) between 100 and 200. On the other hand, MCHENRY JR. and WILHELM (1957) further explored the same concept, assuming the axial distance between mixing cells in a packing bed to be equal to the particle diameter, leading to a Pe_d value of about 2 Re_d approximately equals to 35. The disparity between

these findings may be attributed to experimental conditions, particularly the aspect ratio of the bed. BRENNER (1995) provided a solution to a mathematical model for dispersion in a finite-length beds. His work concluded that the solutions derived by DANCKWERTS (1953) for an input step in solute concentration and LEVENSPIEL and SMITH (1957) for a pulse in solute concentration in a infinite bed are correct for $Pe(= \bar{u}L/4D_L) \geq 10$.

Some researchers proposed correlations to cover ranges of Reynolds numbers. That is the case of HIBY (1962), who presented an improved empirical correlation to encompass Reynolds number ($Re = d_p U_0/\nu$) up to 100, supported by experimental results. SINCLAIR and POTTER (1965) used a frequency-response technique to study the flow of air through beds of glass spheres within a Reynolds number ($= dU/\nu$) range from 0.1 up to 20. EVANS and KENNEY (1966) extended this investigation into the intermediate Reynolds number region ($53 < Re = dU/\nu < 1587$) using a pulse response technique in beds of glass spheres and Raschig rings.

For almost all studies, the boundary conditions correspond to the semi-infinite bed, which mathematically means that the ratio between the length and diameter of the experimental column must be higher than 20, $L/D > 20$. The empirical studies showed that the longitudinal dispersion coefficient has a functional dependence on many parameters, such as column length and diameter, the inflow velocity, particle diameter, molecular diffusion coefficient of the solute, and density and viscosity of the liquid.

2.2 Transverse dispersion

2.2.1 Experimental studies

Typically, most investigators measure the transverse dispersion coefficients in non-reactive conditions because the mass transfer rate correlates to the transverse dispersion in porous media and packed beds. The prevailing method for assessing transverse dispersion involves introducing a continuous tracer stream from a local

source within the bed, typically positioned along the axis, and gauging the radial fluctuation in tracer concentration at one or more downstream sites.

TOWLE and SHERWOOD (1939) were the first investigators to explore the radial dispersion in a gaseous system. Their findings were pivotal for understanding packed-bed dispersion as they revealed that tracer molar mass did not influence dispersion. In liquid systems, BERNARD and WILHELM (1950) conducted experiments to measure the transverse coefficient in packed beds using the Fickian model. Their experiments, factoring in the wall effect condition, indicated that at high Re numbers, the value of the transverse dispersion coefficient is constant. On the other side, BARON (1952) proposed a novel model of radial dispersion wherein a tracer particle undergoes a simple random walk displacement whose length is the radius of the packed bed particles, yielding a transversal Péclet number, ($Pe_t = \bar{u}d_p/D_t$), between 5 and 13 once $Re(= Ud_p/\nu) \to \infty$. This prediction stems from the random-walk theory, employing a statistical approach that disregards radial variations in velocity in void space. Later, LATINEN (1951) expanded the random-walk concept to three dimensions, projecting a $Pe_t = 11.3$ when Reynolds numbers approximate to infinity value.

KLINKENBERG A. (1953) addressed anisotropic dispersion through the solution of the solute transport equation, albeit within the framework of an infinite medium. Their study also encompassed cases of isotropic dispersion, where the longitudinal and transverse coefficients have the same value. On the other hand, DORWEILER and FAHIEN (1959) used the solution in terms of Bessel functions formulated by FAHIEN and SMITH (1955) for macroscopic models to measure the mass transfer in both laminar ($Re_{d_p}(= ud_p/\nu) < 200$) and transient flow ($200 < Re_{d_p}(= ud_p/\nu) < 1200$ regimes in packed column. Their finding showed a linear correlation between the fluid velocity and the transverse Péclet number ($= DU_s/E$) for $Re_{d_p}(= ud_p/\nu) < 200$. However, when $Re_{d_p} > 200$, this Péclet number seemed constant at room temperature. These authors also showed that the transverse Péclet($= ud_p/D_t$) achieved a constant value from the axis about 80% if

the packed-column radius and then changed while the wall region was approximated.

SAFFMAN (1959) considered the packed bed as a network of capillary tubes that are randomly orientated concerning the main flow. For infinitely long times and high Reynolds number ($= Ul/\nu$), he showed that with the assumption of stagnated fluid at the capillary walls, the time needed for a tracer particle to leave the capillary would be infinite as its distance from the walls goes to zero. Moreover, ROEMER *et al.* (1962) studied radial mass transfer considering low flow rates, hence $Re(= d_pG/\mu) < 100$. The authors concluded that if longitudinal dispersion is neglected in calculating the transverse dispersion coefficient, for typical values of Re between 10 and 20, D_T can be in error up to 10% of error.

One of the primary methods for calculating the transverse dispersion coefficient involves plotting the 10% or 90% composition of the initial tracer concentration (specifically C_{10} and C_{90}) against the distance until to achieve 50% of the initial composition. Additionally, the continuous point source and instantaneous finite source techniques are commonly used for experimentally measuring the transverse dispersion coefficient. However, a novel experimental technique created by COELHO and DE CARVALHO (1988) enables the measurement of the dissolution rate of planar or cylindrical surfaces with inert particles where the fresh fluid flows in axial direction. This innovative approach allows predicting the transverse dispersion coefficient value based on mass transfer measurement.

2.2.2 Instantaneous finite source method

Several authors, including DORWEILER and FAHIEN (1959), FAHIEN and SMITH (1955), employed an experimental technique that involves introducing a tracer into the column's axis. The analytical model for an instantaneous finite source in one dimension was initially introduced by CRANK (1979), which was later expanded by BAETSLE (1969) to encompass three-dimensional dispersion. HUNT (1978) SUN and SUN (2014) provided three-dimensional solutions to the advection-dispersion equation using distinct mathematical analyses. Furthermore, VAN GENUCHTEN

(1982) contributed with numerous analytical solutions to the one-dimensional convective-dispersive solute transport equations. The instantaneous finite-source technique requires careful attention to some details to ensure accurate results, as tracer concentration must remain sufficiently low to mitigate density-induced flow effects. Additionally, the tracer must be conserved throughout the experiment, and the outlet's flow rate distribution should mirror that of the feed to prevent complications in the flow field, such as recirculation and flow stagnation.

2.2.3 Continuous point source method

This technique measures mass transfer between two coaxial segments of a packed bed. Liquid flows parallel to the axis, with the central portion fed with a small flow rate with sodium chloride and the outer segment receiving pure water. Previous studies, such as those by KLINKENBERG *et al.* (1953), neglected the effect of injector radius when formulating the steady-state solution for the solute transport equation. Other researchers, such as PLAUTZ and JOHNSTONE (1955), SINCLAIR and POTTER (1965), developed analytical solutions for mass diffusion from a point source with no boundaries. Many investigators have explored different boundary conditions, each proposing analytical solutions.

2.2.4 Mass transfer from a flat surface aligned with the flow

In a more recent study, COELHO and DE CARVALHO (1988) introduced a novel approach for determining the transverse dispersion coefficient. Their methodology involves measuring the dissolution rates of certain species, assuming that the liquid flow is steady with a uniform average interstitial velocity and that the column walls are saturated with this solute. Their analytical solution demonstrated a direct correlation between the measurement of the solid's dissolution rate and the transverse dispersion coefficient in the bed. Their research results are striking compared to those of HIGBIE (1935).

2.2.5 Numerical simulations

Several studies (BABAEI and JOEKAR-NIASAR, 2016; BIJELJIC and BLUNT, 2007; BIJELJIC *et al.*, 2004; BRUDERER and BERNABÉ, 2001; KOHNE *et al.*, 2011; MEHMANI *et al.*, 2014) have investigated solute transport using Pore Network Models (PNM) mainly under the laminar Darcy flow regime. PNM offers a significant advantage in computational efficiency over other methods, such as LBM or DNS. This efficiency allows dispersion simulations across larger domains (2D or 3D) to achieve an asymptotic state.

For instance, when analysing their pore-network models, KOHNE *et al.* (2011) and BABAEI and JOEKAR-NIASAR (2016) implemented the mixed cell method (MCM). Meanwhile, BRUDERER and BERNABÉ (2001) utilised PNM to obtain longitudinal and transverse dispersion coefficients for 2D pore networks that exhibit varying levels of heterogeneity. Their approach involved using a discrete random walk method to model molecular diffusion and applying the spatial moment's analysis to determine both dispersion coefficients for each simulation. Their results showed a power law relationship between D_L and the Péclet number. However, their findings for transverse dispersion did not align with existing literature, revealing a weak correlation between D_T and the velocity or Péclet number.

BIJELJIC *et al.* (2004) and BIJELJIC and BLUNT (2007) investigated the properties of asymptotic longitudinal and transverse dispersion coefficients in 2D pore networks with a diamond lattice of pore throats connected by volumeless pores. They introduced heterogeneity to the lattice by varying the pore throat radii, mimicking Berea sandstone's size distribution. Their findings indicated that when the Péclet number ($= \bar{u}L/D_m$) was more significant than 1, a power law pattern was observed in the relationship between the ratio of the transverse dispersion and molecular diffusion coefficients and $Pe = \bar{v}L/D_m$.

When examining dispersion in porous media, monitoring the time or length required to reach the asymptotic regime is crucial. As solute enters a porous medium, the dispersion coefficient gradually changes until it stabilises at a constant value.

According to BIJELJIC and BLUNT (2007), an asymptotic dispersion occurs when the solute fully interacts with the velocity field within the medium. It is worth noting that the length required to achieve the asymptotic regime for transverse dispersion is significantly shorter than that for longitudinal dispersion. Furthermore, the asymptotic length increases with the Péclet number. In the 2D pore networks studied by BIJELJIC and BLUNT (2007), fewer transversed pores were required to reach asymptotic $\mathcal{D}_{vt} = D_T/D_m$ values compared to $\mathcal{D}_v = D_L/D_m$, where $\mathcal{D}_{vt}$ and $\mathcal{D}_v$ are the dimensionless transverse and longitudinal dispersion coefficients, respectively. For D_L, the asymptotic length varied from one pore length in the diffusion-dominated regime ($0 < Pe < 1$) to 100 or 1000 pores at higher Pe, while for D_T, it ranged from one pore length in the diffusion-dominated regime to 10 or 20 pores at higher Pe, where $Pe = \bar{v}L/D_m$.

ACHARYA *et al.* (2007) studied the transverse dispersion in a 2D porous media by LBM simulations. They found that asymptotic D_T values were attained after travelling distances ranging from 10 to 80 grain diameters. Similarly, MAIER *et al.* (2000) explored longitudinal and transverse dispersion in 3D regular and random sphere packings using LBM simulations and Nuclear Magnetic Resonance (NMR) experiments. Their results indicated that asymptotic D_L values were achieved after travelling an asymptotic length of 3 sphere diameters, while asymptotic D_T values were observed after a length of 1.34 sphere diameters for all Péclet values.

In a recent study, MACHADO *et al.* (2023) introduced a new technique called sub-volume analysis (SVA) to extract macroscopic model parameters and their uncertainties from pore-scale simulations using the PNM approach. The researchers employed SVA to compute the longitudinal dispersion coefficient of the advection-dispersion model (ADM) from continuous tracer injection problems. The findings showed the minimum network length required to reach an asymptotic dispersion regime where the ADM can be applied. Furthermore, the methodology was tested on various statistically constructed networks and on those built from microtomographies of a Berea sandstone sample. The results demonstrated a remarkable level

of agreement within the error margins for the asymptotic longitudinal dispersion coefficient for pore networks of the same type in different realisations and also when compared with other methods, such as breakthrough curve and moments method. This promising technique has sparked further exploration into the potential of SVA to determine not only the longitudinal dispersion coefficient but also the transverse dispersion coefficient.

Chapter 3

Methodology

This section aims to present the developed methodology used in the current work, which describes the dispersion phenomena, the macroscopic dispersion model in porous media and its analytical solutions, the pore-network dispersion model and the sub-volume analysis (SVA) used to analyse its results determining the D_L (or $\mathcal{D}_v$) and, lastly, the D_T (or $\mathcal{D}_{vt}$) by a estimation process.

3.1 Dispersion in porous media

The most popular method of defining a macroscopic dispersion model, according to BATTIATO *et al.* (2019), is scaling up the conservation's law from the pore scale. The advection-dispersion equation arises as derived by WHITAKER (1999), after selecting a Representative Elementary Volume (REV) and applying the Volume Averaging Method (VAM) to the REV for the passive solute transport in a single uncompressible phase through a saturated porous media. The advection-dispersion model is given by

$$\frac{\partial C}{\partial t} + \mathbf{v} \cdot \nabla C = \nabla \cdot [\mathbf{D} \cdot \nabla C] \tag{3.1}$$

where C, $\mathbf{v}$ e $\mathbf{D}$ are the mean concentration per unit of fluid volume, the mean intrinsic velocity vector and the dispersion tensor, respectively.

For an isotropic domain, it can be shown that the dispersion tensor becomes a diagonal matrix (SALLES *et al.*, 1993) when $\mathbf{D}$ is expressed in Cartesian coordinates with its first coordinate aligned with the $\mathbf{v}$ direction, as given by:

$$\mathbf{D} = \begin{bmatrix} D_L & 0 & 0 \\ 0 & D_T & 0 \\ 0 & 0 & D_T \end{bmatrix} \tag{3.2}$$

where D_L and D_T are the longitudinal and transverse dispersion coefficients. The experimental determination of D_L is usually performed through the transient bulk concentration at the outlet, known as the breakthrough curve. There are other experimental methods like the works of DE CARVALHO and DELGADO (2000) and ROBBINS (1989) to determine D_T.

3.2 Dispersion in macroscopic models

Let us consider a porous media with porosity ε, length L, height $2B$, with fresh fluid injected by the left side with superficial velocity $\mathbf{u} = u\hat{\mathbf{e}}_x = \epsilon\mathbf{v} = \epsilon v\hat{\mathbf{e}}_x$, with solute concentration equals to C_{in} at the injection boundary and to C_w at the top and bottom walls as shown in Figure 3.1.

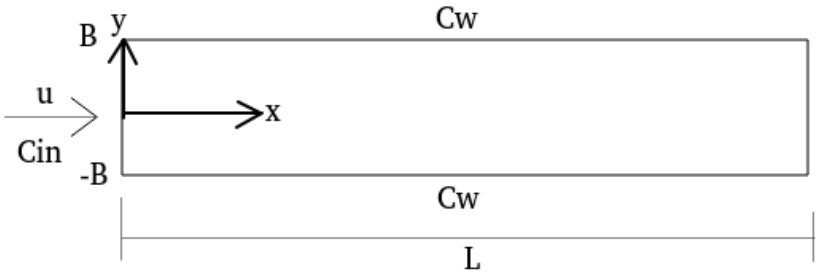

Figure 3.1: 2D domain sketch.

For the steady state in a 2D domain, Eq. 3.1 can be reduce to the macroscopic

advection-diffusion equation given by:

$$u\frac{\partial C}{\partial x} - \epsilon D_T \frac{\partial^2 C}{\partial y^2} - \epsilon D_L \frac{\partial^2 C}{\partial x^2} = 0 \tag{3.3}$$

.

Equation 3.3 can be made dimensionless by using

$$\eta = \frac{y}{B},\ \zeta = \frac{x}{B},\ \phi = \frac{C - C_w}{C_{in} - C_w},\ Pe_L = \frac{uL}{\epsilon D_L} = \frac{vL}{D_L},\ A = \frac{L}{B},\ R = \frac{D_L}{D_T} \tag{3.4}$$

where $\eta, \zeta, \phi, Pe_L, A$ and R are the dimensionless transversal and longitudinal coordinates to the flow, the dimensionless concentration, the Péclet number related to the longitudinal dispersion coefficient, the ratio between the length of the domain and its half height, and the ratio between the longitudinal and transverse dispersion coefficients, respectively, and being ε its porosity. Using this variables, Equation 3.3 is written as:

$$Pe_B \frac{\partial \phi}{\partial \zeta} - R\frac{\partial^2 \phi}{\partial \zeta^2} = \frac{\partial^2 \phi}{\partial \eta^2} \tag{3.5}$$

where $Pe_B = uL/\varepsilon D_T = vL/D_T$ and the Equation 3.5 must satisfy the following boundary conditions:

$$\begin{aligned} \zeta = 0, &\quad \phi = 1 \\ \eta = 1, &\quad \phi = 0 \\ \eta = 0, &\quad \frac{\partial \phi}{\partial \eta} = 0 \end{aligned}$$

and another one for the ζ direction, which can be stated as

$$\zeta \to \infty, \quad \phi = 0, \tag{3.6}$$

or

$$\zeta = A, \quad \frac{\partial \phi}{\partial \zeta} = 0 \tag{3.7}$$

to infinite and finite domains, respectively. The mean dimensionless concentration in the cross-section area is given by:

$$\bar{\phi}(\zeta) = \int_0^1 \phi(\zeta, \eta) d\eta \tag{3.8}$$

whose solution using the boundary condition given by Equation 3.6 is:

$$\bar{\phi}(\zeta) = \sum_{n=0}^{\infty} \frac{2}{\lambda_n^2} \exp\left\{ \frac{Pe_B}{2R} \zeta \left[1 - \left(1 + \frac{4R\lambda_n^2}{Pe_B^2} \right)^{1/2} \right] \right\} \tag{3.9}$$

while, for the boundary condition given by 3.7, the solution is:

$$\bar{\phi}(\zeta) = \sum_{n=0}^{\infty} \frac{2}{\lambda_n^2} \left[\frac{\exp(r_{2n}\zeta) - \left(\frac{r_{2n}}{r_{1n}} \right) \exp\left[A(r_{2n} - r_{1n}) + r_{1n}\zeta \right]}{1 - \left(\frac{r_{2n}}{r_{1n}} \right) \exp[(r_{2n} - r_{1n})A]} \right] \tag{3.10}$$

where r_{1n} and r_{2n} are the positive root and the negative roots, and λ_n are the eigenvalues of the eigenproblem derived from the partial differential equation, being defined as follow:

$$r_{1n} = \frac{Pe_B}{2R} \left[1 + \left(1 + \frac{4R\lambda_n^2}{Pe_B^2} \right)^{1/2} \right], \tag{3.11}$$

$$r_{2n} = \frac{Pe_B}{2R} \left[1 - \left(1 + \frac{4R\lambda_n^2}{Pe_B^2} \right)^{1/2} \right], \tag{3.12}$$

$$\lambda_n = \pi \left(n + \frac{1}{2} \right) \tag{3.13}$$

Annexe A provides a detailed deduction of the analytical solutions.

3.3 Dispersion in pore-network models

SAHIMI (2011) stated that the solute transport equation, which describes the dispersion during injection at the pore scale, can be written as:

$$\frac{\partial c}{\partial t} + \mathbf{U} \cdot \nabla c = \nabla \cdot (D_m \nabla c) \tag{3.14}$$

where c is the concentration at the pore scale, $\mathbf{U}$ is the fluid velocity vector in the porous space, and D_m is the solute molecular diffusion coefficient. The integration of Equation 3.14 over the effective pore volume, V_i^{eff}, followed by the application of the divergence theorem, gives:

$$V_i^{eff} \frac{\partial c_i}{\partial t} = -\sum_{j=1}^{Z_i} \dot{m}_{ij} \tag{3.15}$$

where V_i^{eff} is the sum of the volume of pore i and the halves of all throat volumes connected to it, c_i is the mean solute concentration in V_i^{eff}, Z_i is the coordination number which represents the number of pores connected to pore i through throats, and $\dot{m}_{ij}$ is the net mass flow rate that is transported by diffusion and advection from pore i to pore j. For the pore network model, the inlet condition is the injection of fluid with zero solute concentration by advection.

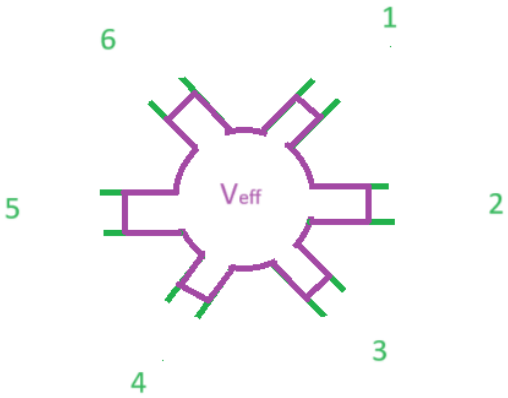

Figure 3.2: Effective pore volume.

For the steady-state incompressible flow of a Newtonian fluid, the flow from pore

i to pore j can be given by:

$$q_{ij} = g^h_{c,ij} \left(p_i - p_j\right) \tag{3.16}$$

where $g^h_{c,ij}$ is the hydraulic conductance of the conduit between pores i and j, p_i and p_j are the pressures values at pores i and j, respectively. $g^h_{c,ij}$ takes into account the conductance of the throat that connects pores i and j and the conductance of halves of these pores, and it can be calculated as:

$$g^h_{c,ij} = \left(\frac{1}{g^h_i} + \frac{1}{g^h_{ij}} + \frac{1}{g^h_j}\right)^{-1} \tag{3.17}$$

which g^h_i, g^h_j and g^h_{ij} represents the hydraulic conductances of the halves of the pores i, j and the throat that connects them. It is important to highlight that these conductances become defined by applying the Hagen-Poiseuille equation to Equation 3.17. If considering pores as spheres and throats as cylinders, the hydraulic conductances of the throat connecting pores i and j can be calculated by:

$$g^h_{ij} = \frac{\pi}{128\mu}\left(\frac{d^4_{ij}}{l_{ij}}\right) \tag{3.18}$$

where d_{ij} and l_{ij} is the throat diameter and throat length connection pores i and j. The g^h_i and g^h_j are calculated similarly, but replacing $l_i = d_i/2$ and $l_j = d_j/2$.

The net volumetric flow rate at all pores of the network must be zero due to volume conservation, which means that (GOSTICK *et al.*, 2016):

$$Q = \sum_{j=1}^{Z_i} g^h_{c,ij} \left(p_i - p_j\right) = 0, \quad i = 1, 2, ..., N_p \tag{3.19}$$

where N_p is the total number of pores in the pore network, and the index j is the index of a pore connected to of pore i. Equation 3.19 is a sparse linear system, whose solution provides the pressure at the network pores. Once the pressure is

found for each pore, one can use Equation 3.16 to calculate the flow rates, q_{ij}, at all conduits.

3.4 The sub-volume analysis (SVA)

Recently, MACHADO *et al.* (2023) developed a new methodology to use volume-averaged data from the pore-network simulations to estimate parameters values and their uncertainties for macroscopic models. The sub-volumes are domains within the pore network, which can be understood as a slab perpendicular to the flow but with a small thickness in the flow direction. The superposition of slabs centred in nearby axial positions defines a moving averaging window. The dimensionless sub-volume thickness is determined $\mathcal{L} = l_v/l_{pp}$, where l_v and l_{pp} are the sub-volume thickness and pore-to-pore distance, which is illustrated in Figure 3.3.

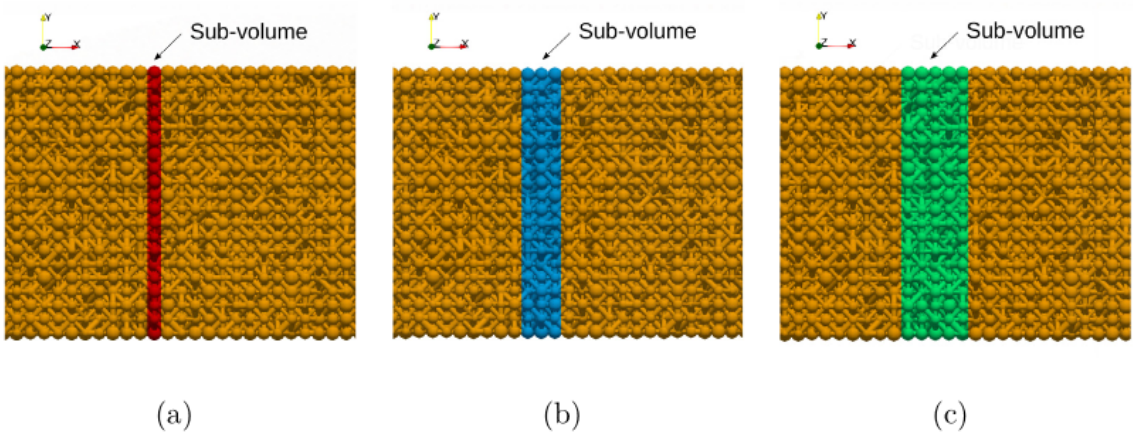

Figure 3.3: Sub-volumes with $\mathcal{L}$ equal to (a) 1, (b) 3 and (c) 5 in a pore network. Reproduced from MACHADO *et al.* with permission.

This methodology allows us to estimate the dimensionless longitudinal dispersion coefficient, $\mathcal{D}_v$, and its error at the 95% confidence level. Similarly, the present work aimed to estimate the dimensionless transverse dispersion coefficient, $\mathcal{D}_{vt}$, and its error at 95% confidence level, $e_{95}(\mathcal{D}_{vt})$, as an extension of the SVA methodology. For this, as in the work of MACHADO *et al.* (2023), the volume-averaged solute concentration, $\langle c_p \rangle_V^{(k)}$, at all k sub-volume barycenter positions, $\langle x_p \rangle_V^{(k)}$, should represent the cross-area averaged solute concentration profile along the domain. Moreover,

the standard deviation of the solute concentration, $\sigma\left(\langle c_p\rangle_V^{(k)}\right)$, and the barycenter position error, $\Delta\langle x_p\rangle_V^{(k)}$, were used to measure the effect of the domain on the determination of $\mathcal{D}_v$ and $\mathcal{D}_{vt}$.

For $\mathcal{L} > 1$, the sub-volume thickness increases equally in both directions, upstream and downstream, generating overlapping sub-volumes. The barycenter position in x direction of each sub-volume is described by:

$$\langle x_p\rangle_V^{(k)} = \frac{\sum_{i=1}^{n_p^{(k)}} x_{i,p} V_{p,i}^{V_{p,i}^{eff}}}{\sum_{i=1}^{n_p^{(k)}} V_{p,i}^{V_{p,i}^{eff}}} \tag{3.20}$$

where $n_p^{(k)}$ is the total number of pores in the sub-volume k, and $x_{p,i}$ is the barycenter of pore i. The error in the determination of the barycenter position was estimated using:

$$\Delta\langle x_p\rangle_V^{(k)} = \left|\langle x_p\rangle_V^{(k)} - \langle x_p\rangle_V^{(m)}\right| \tag{3.21}$$

where $\langle x_p\rangle_V^{(m)}$ is calculated analogously to $\langle x_p\rangle_V^{(p)}$, just replacing p to m. The sub-volume m has one more layer of pores in both the left and right directions when compared with the sub-volume k. Similar to the barycenter position calculation, the volume-averaged solute concentration in the sub-volume k can be calculated using the following equation:

$$\langle c_p\rangle_V^{(k)} = \frac{\sum_{i=1}^{n_p^{(k)}} c_{p,i} V_{p,i}^{eff}}{\sum_{i=1}^{n_p^{(k)}} V_{p,i}^{eff}} \tag{3.22}$$

In addition, the standard deviation of the solute concentration for the pores within a sub-volume comes from:

$$\sigma\left(\langle c_p\rangle_V^{(k)}\right) = \sqrt{\frac{1}{n_p^{(k)}} \sum_{i=1}^{n_p^{(k)}} \left(\langle c_p\rangle_V^{(k)} - c_{p,i}\right)^2} \tag{3.23}$$

3.5 Longitudinal and transverse dispersion coefficient estimation

In order to determine $\mathcal{D}_v$, at a given time t, $\mathcal{L}$ is considered adequate when α does not vary by more than 1% if its value for a further increase in $\mathcal{L}$, where α is the standard deviation, of the $\sigma\left(\langle c_p\rangle_V^{(k)}\right)$ (see details in MACHADO *et al.*, 2023). On the other hand, because of the steady-state nature of the present work, $\mathcal{L}$ is adequate when the values of $\mathcal{D}_{vt}$ and its 95% confidence error does not vary more than 1%.

To estimate the dimensionless longitudinal dispersion coefficient, at a given time instant, t, the volume-averaged values of $\langle c_p\rangle_V^{(k)}$ and $\langle x_p\rangle_V^{(k)}$ with their respective error estimates are calculated and it is assumed that $\langle c_p\rangle_V^{(k)}$ and $\langle x_p\rangle_V^{(k)}$ represents the solute distribution in time and position, $\bar{C}(x,t)$. So D_L, can be estimated by adjusting the analytical solution to the data extracted from the pore-network simulation. The reader can find more details of the SVA and its application to determine D_L in the original work of MACHADO *et al.* (2023).

A complementary methodology was developed for the D_T determination. One can realise that the analytical solution for $\bar{\phi}(\zeta)$ depends on the R parameter, which represents D_L/D_T, in other words, the method is valid once the value of D_L is obtained using the SVA methodology. Another difference is the usage of a solution for the steady-state, as mentioned before, which means that the sub-volumes' solute concentrations at their barycenter positions represent the solute distribution along the flow direction, which can be used together the analytical solution to determinate R, and, thus, D_T. Several simulations were performed to verify the influence of the length and height of the domain on the value of D_L and D_T, for a few Péclet (Pe_m) numbers. Each pore network was statistically built 10 times and then the mass transport simulation was performed in each one, to verify the range of D_L values among them.

For both dispersion coefficients, two different types of averages were performed. First, for a set of realisations, $\langle\mathcal{D}_{vt}\rangle \pm e_{95}(\langle\mathcal{D}_{vt}\rangle)$ were calculated, which are the mean

values to the transverse dispersion coefficient and its error at 95% confidence level. Secondly, taking the values of the transverse dispersion coefficient and their errors for each realisation and adjusting them to a constant function, we can obtain the $\bar{\mathcal{D}}_{vt} \pm e_{95}(\bar{\mathcal{D}}_{vt})$.

Chapter 4

Numerical Procedure

All the simulations and analytical solutions implemented in this work and the open-source codes used were written or accessed via Python. The OpenPNM version 2.6.0, developed by GOSTICK *et al.* (2016) uses the Numpy v1.20.3 and Scipy v1.6.3 libraries, which were developed by HARRIS *et al.* (2020) and VIRTANEN *et al.* (2020), respectively. OpenPNM was used to build the pore networks and simulate the flow and the solute transport process. A Python routine using the OpenPNM library calculated the sub-volume properties.

4.1 Implementation of the finite and semi-infinite solutions

The ζ values were defined within $[0, 1 - A]$ with equidistant intervals of 0.1 and $A = 10$. The A value was chosen in accordance with the analytical solutions' behaviour in order that $\bar{\phi} \to 0$ but with a clear picture of their exponential decay. Thus, we could compare the two analytical solutions. Since $D_T \leqslant D_L$, the R values were defined as 1, $10^{0.5}$ and 10. The Pe_L values were set to 0.01, 0.1 and 1. The absolute error of the series solutions, Equations 3.9 and 3.10 at each point $\zeta_i = 0.1i$ $(i = 1, 2, ..., N_\zeta = 100)$, where N_ζ is the number of points within the ζ interval, was calculated according to:

$$\delta(\zeta_i) = \left|\bar{\phi}(\zeta_i)_f - \bar{\phi}(\zeta_i)_{f-1}\right| \tag{4.1}$$

where $\bar{\phi}(\zeta_i)_f$ represents the sum of the values of the series terms up to $n = f$ at ζ_i until the absolute error criteria achieves a value lower than 10^{-4}. On the other hand, $\bar{\phi}(\zeta_i)_{f-1}$ is the sum of series' terms up to $n = f - 1$ at ζ_i. Once the absolute error at all points are known, the maximum absolute error, $\delta_{\max}$, and mean absolute error, $\bar{\delta}$, can be calculated by:

$$\delta_{\max} = \max_{i=1,\ldots,N_\zeta} [\delta(\zeta_i)] \quad \text{and} \quad \bar{\delta} = \frac{1}{N_\zeta}\sum_{i=1}^{N_\zeta} \delta(\zeta_i) \tag{4.2}$$

The 95% confidence error of $\bar{\phi}$ can be calculated as follow:

$$e_{95\%}(\bar{\phi}) = \frac{t_{95\%_{n_p-1}}}{\sqrt{n_p}}\sigma(\bar{\phi}) \tag{4.3}$$

where n_p is the number of porous contained in each sub-volume, $\sigma(\bar{\phi})$ the standard deviation of the mean dimensionless concentration and $t_{95\%_{n_p-1}}$ is the value of t-student with the confidence level of 95% which approaches 1.96 when $n_p \to \infty$.

4.2 Pore network construction

Porous media are investigated using two different types of cubic-network models: Simple cubic lattice and multi-directional connectivity pore network in a cubic lattice. The former has pores with a coordination number equal to 6, the latter has pores with a coordination number equal to 26 with random elimination of 30% of pores and throats connected to them. The pores are characterised as spherical and are connected to each other by cylindrical throats with circular cross-sections. MACHADO *et al.* (2023) implemented using OpenPNM an algorithm to build statistically-defined cubic lattice pore networks with prescribed petrophysical

properties, those can be found in Table 4.1, where L_x, L_y and L_z are the length of the domain in x, y and z directions, respectively, ε is the porosity, K_x is the permeability in the x direction, N_p is the total number of pores in the pore network and L_{pp} is the distance between two pores. The networks with (*) symbol mean that were built by MACHADO *et al.* (2023).

Table 4.1: Properties of statistically built pore networks.

Network	N_p	$L_{pp}(mm)$	L_x(mm)	L_y(mm)	L_z(mm)	$\varepsilon(\%)$	$K_X(D)$
$C1^*$	200 000	0.5	250	10	10	39.96	100.4
$C3^*$	600 000	0.5	750	10	10	39.98	100.4
$C4^*$	800 000	0.5	1000	10	10	39.99	100.4
$C4_{2h}$	1 600 000	0.5	1000	20	10	39.97	100.4
$CZ1^*$	112 546	0.1	40	2	2	29.87	1.013
$CZ3^*$	338 154	0.1	120	2	2	29.90	1.013
$CZ4^*$	450 618	0.1	160	2	2	29.90	1.013
$CZ4_{2h}$	905 578	0.1	160	4	2	29.93	1.013

To construct cubic-lattice pore networks, we utilised the Permuted Congruential Generator method (O'NEILL, 2014) from the Numpy library to generate pseudo-random numbers. These numbers were essential for reducing mean coordination numbers by randomly eliminating pores and throats and determining pore and throat diameters based on a prescribed distribution. The size of pores and throats in all networks is determined by a statistical distribution algorithm, which is tailored to attain the desired values of porosity and permeability for each network. For the simple cubic network, MACHADO *et al.* (2023) outlined the algorithm in their work, which is provided below.

1. Read the prescribed properties: porosity, permeability, coordination number, the averaged distance between pores, and network lengths: L_x, L_y and L_z.

2. Define first guesses for the mean pore and throat diameters using approximated correlations based on the porous media representation as a bundle of capillarity

tubes connecting the inlet and outlet of the sample, where we used the Hagen-Poiseuille and Darcy equations.

3. A cubic pore network is built with a coordination number equal to 6 for all pores.

4. Define all pore-network geometry entities considering a normal distribution of pore and throat diameters, using the estimates obtained in step 2 as mean values for pore and throat diameters.

5. Minimize the absolute difference between the prescribed and calculated porosity value by tweaking the pore diameter distribution's mean value until reaching a defined tolerance.

6. Minimize the absolute difference between the prescribed and calculated permeability value by tweaking the mean value of the throat diameter distribution until it reaches a defined tolerance.

7. Repeat steps 5 and 6 as many times as necessary.

The steps for a multi-directional connectivity pore network in a cubic lattice are almost the same as the simple cubic. However, the step 3 was replaced by the steps below:

- Build a cubic pore network with a coordination number equal to 26 for all pores.

- Randomly remove 30% of pores and throats connected to them.

- Adjust the averaged coordination number by randomly eliminating throats. However, preserve all throats belonging to the sample-spanning cluster.

4.3 Flow and tracer transport simulation

4.3.1 Flow conditions

To determine the flow field of the network, a constant volumetric flow rate at the inlet boundary was imposed using the pressure difference between inlet and outlet boundaries, ΔP. The following equation defines the microscopic Péclet number:

$$Pe_m = \frac{v_x|_{x=0} L_{pp}}{D_m} \tag{4.4}$$

The Darcy equation can used to determine the pressure difference that gives the outlet value of the intrinsic velocity

$$\Delta P = \frac{v_x|_{x=0} \varepsilon \mu L_x}{K_X} \tag{4.5}$$

where μ is the viscosity of the fluid. Combining in Equations 4.5 and 4.4, one can easily obtain the pressure difference between inlet and outlet by:

$$\Delta P = \frac{Pe_m D_m}{L_{pp}} \frac{\varepsilon \mu L_x}{K_X} \tag{4.6}$$

Once the Pe_m value is fixed and the other parameters are known, the pressure difference between the inlet and outlet boundaries is calculated and imposed as boundary conditions. Then, the algorithm *StokesFlow* from the OpenPNM code was performed to solve the sparse linear system of the pressure field, given by Equation 3.19, allowing to determine the flow rate in each throat from Equation 3.16 and, consequently, the flow field. The sparse linear system within the Stokes Flow algorithm was solved with a relative tolerance of 10^{-10} by the PARDISO library, developed by SCHENK *et al.* (2001) and accessed via PyPardiso version 0.4.1 (HAAS and SROCKA, 2023).

4.3.2 Tracer transport conditions

Once the flow field is known, the mass transport inside the pore network could be performed. Two different algorithms were used, one to determine D_L and other to determine D_T. The former was performed with a transient solver, *TransientAdvectionDiffusion*, and the latter with a stationary solver, *AdvectionDiffusion*. The species conservation equation at steady-state for an arbitrary pore i is given by the simplification of Equation 3.15 as:

$$\sum_{j=i}^{z_i} \dot{m}_{ij} = 0 \tag{4.7}$$

To perform the steady-state tracer transport, the stationary algorithm was settled up with a relative tolerance of 10^{-8} for the pores' concentrations. The top and bottom walls were saturated with solute, while the inlet and outlet had no solute. The pores at the outlet boundaries allowed no solute accumulation to enforce a boundary condition compatible with Equation 3.7. Further, there were no normal flow at the other boundaries that are kept saturated. The reader can find more information about the transient solver and its numerical procedure to determine D_L in the work of MACHADO *et al.* (2023).

4.4 SVA application to determine the longitudinal dispersion coefficient

To determine the longitudinal dispersion coefficient, at a given time t, of the transient mass transfer process, we calculated the volume-averaged values of $\langle c_p \rangle_V^{(k)}$ and $\langle x_p \rangle_V^{(k)}$, with their respective errors estimates for all sub-volumes k with thickness $\mathcal{L}$ in the domain. Assuming that $\langle c_p \rangle_V^{(k)}$ and $\langle x_p \rangle_V^{(k)}$ represent the distribution of solute in time and space in the macroscopic model, we could estimate D_L by adjusting the analytical solution to these data. Furthermore, other input data were needed during the procedure, including the network properties described in Table 4.1. The estima-

tion of D_L was performed using the ODRPACK, where, according to MACHADO *et al.* (2023), the relative tolerance for all fitting curves were 10^{-20} and 10^{-25} for the convergence of the sum of squares and the estimated parameter, respectively. The ODR (Orthogonal Distance Regression) package differs from normal regression as takes into account the determination errors for both independent and dependent variables.

Once D_L is estimated at each time t, their values were analysed by plotting the dimensionless longitudinal coefficient, $\mathcal{D}_v = D_L/D_m$, and their errors using the 95% confidence interval, $e_{95}(\mathcal{D}_v)$, versus the dimensionless time, $T = v_x t/L_x$. If the domain is long enough, the asymptotic dispersion regime is reached somewhere within $0.4 < T < 0.8$, where $\mathcal{D}_v$ tends to a constant value. However, if the length is not long enough, $\mathcal{D}_v$ can be estimated before the tracer advancing front reaches the domain outlet (MACHADO *et al.*, 2023), but it would not be the asymptotic value.

Therefore, when the $\mathcal{D}_v(T)$ remains nearly constant within a certain T range, we can use its value and uncertainties to determine the dimensionless dispersion coefficient, $\bar{\mathcal{D}}_v^{(\Delta t)}$, and its uncertainty in the asymptotic regime by adjusting a constant function over the T interval. Additionally, we can estimate an average value for the dimensionless longitudinal coefficient and its uncertainty for a set of realisations using differents procedures (see details MACHADO *et al.*, 2023).

4.5 SVA application to determine the transverse dispersion coefficient

To determine the transverse dispersion coefficient, D_T, after the flow and tracer concentration fields were obtained as described previously, we could extract the values of $\langle c_p \rangle_V^{(k)}$ and $\langle x_p \rangle_V^{(k)}$ and their errors from the pore-network results for different sub-volume thickness. Assuming that $\langle c_p \rangle_V^{(k)}$ and $\langle x_p \rangle_V^{(k)}$ represent the solute distribution in space in the macroscopic model, we could estimate $R = D_L/D_T = \mathcal{D}_v/\mathcal{D}_{vt}$ by adjusting the analytical solution to these data, which tolerance of 10^{-8} was set-

tled up in order to ensure that the values of concentration in each point no longer depend on the value of n, where n is the number of terms needed in the series analytical solution in each point. When ODR was used to estimate R, the $\mathcal{D}_v$ value and pore-network petrophysical parameters were required as input data.

The values of R and its 95% confidence error, $e_{95}(R)$, varied according to the sub-volume thickness, $\mathcal{L}$. Furthermore, the value of R and its error also depends on the amount of data that was used during the estimation procedure using the ODR package, and because of this, a point selection criterion was implemented. The values for $\sigma(\bar{\phi})$ and $\bar{\phi}$ are known for $\zeta \in [0, A]$. In order to narrow down the ζ range utilised for estimating R, a maximum value, ζ_{max}, is selected such that the both the conditions $\bar{\phi} < \bar{\phi}_{min}$ and $\bar{\phi} - 2\sigma(\bar{\phi}) < 0$ are met. Here, $\bar{\phi}_{min}$ is a value close to zero.

The parameters $e_{95}(R)$ and $e_{95}(\mathcal{D}_v)$ represent the 95% confidence error for each parameter, while the 95% error for $\mathcal{D}_{vt}$, $e_{95}\left(\mathcal{D}_{vt}\right)$, can be calculated using the propagation error of R and $\mathcal{D}_v$ as:

$$e_{95}\left(\mathcal{D}_{vt}\right) = \mathcal{D}_{vt}\left[\left(\frac{e_{95}(\mathcal{D}_v)}{D_v}\right)^2 + \left(\frac{e_{95}(R)}{R}\right)^2\right]^{1/2} \tag{4.8}$$

It's noteworthy to recall that $R = D_L/D_T = \mathcal{D}_v/\mathcal{D}_{vt}$.

For a set of realisations, we could also estimate a mean value for the dimensionless transverse dispersion coefficient, $\langle\bar{\mathcal{D}}_{vt}\rangle$, and its error, $e_{95}(\langle\bar{\mathcal{D}}_{vt}\rangle)$. The former could be calculated as

$$\langle\bar{\mathcal{D}}_{vt}\rangle = \frac{1}{N_R}\sum_{i=1}^{r}\mathcal{D}_{vt_i} \tag{4.9}$$

while the latter comes from

$$e_{95}(\langle\bar{\mathcal{D}}_{vt}\rangle) = \frac{1}{N_R}\sum_{i=1}^{r} e_{95}(\langle\mathcal{D}_{vt_i}\rangle) \tag{4.10}$$

where N_R is the total number of realisations, $\mathcal{D}_{vt_i}$ and $e_{95}(\langle\mathcal{D}_{vt_i}\rangle)$ is the dimension-

less transverse dispersion coefficient and its error for the realisation of number i, respectively and r is the maximum value of realisation. Likewise was done for the dimensionless longitudinal dispersion coefficient in the work of MACHADO *et al.* (2023), in this case, the values of $\mathcal{D}_{vt} \pm e_{95}(\mathcal{D}_{vt})$ for a set of realisation were adjusted to a constant function in order to obtain a new value for the dimensionless transverse dispersion coefficient and its error, $\bar{\mathcal{D}}_{vt} \pm e_{95}(\bar{\mathcal{D}}_{vt})$, where this value takes account the error of each realisation. To verify the agreement among realisations' results, a compatibility matrix was used in such way that when the criterion $|\mathcal{D}_{vt,i} - \mathcal{D}_{vt,j}| < e_{95}(\mathcal{D}_{vt,i}) + e_{95}(\mathcal{D}_{vt,j})$ is satisfied, the realisation i is compatible with realisation j. Moreover, the same criterion was used to calculate the percentage of realisations that were in agreement with the value of $\langle \mathcal{D}_{vt} \rangle$.

Chapter 5

Results and Discussion

This chapter aims to compare the results of the two analytical solutions, regarding the effect of R in the $\bar{\phi}$ profiles, the usage of SVA to estimate D_T, and the influence of the domain's height and length to determine R and D_T. Moreover, the variation of the estimated D_T for different network realisations is described as well.

5.1 Comparing the solutions for the finite and semi-infinite domains

For fixed Pe_L, the values of $\bar{\delta}$ and $\delta_{\max}$ for both solutions and chosen values of A, Pe_L and R are shown in Table 5.1, which also provides the mean, Δ, and maximum values, Δ_{max}, of these differences. The solutions agree well except for $Pe_L = 10$, when $\delta_{\max} > 0.003$. Table 5.2 shows $\bar{\delta}$, $\delta_{\max}$, Δ and Δ_{max} for fixed value of Pe_B where the finding reveals that the highest disparity between the series solutions remained below 0.0054. Such differences do not support the usage of the semi-infinite domain solution for the $\mathcal{D}_{vt}$ estimation. Therefore, we used the finite domain solution for all other analyses.

Table 5.1: Mean and maximum absolute percentage errors for series solutions and the difference between the solutions.

Parameters			Finite domain solution		Semi-infinite domain solutions		Absolute difference between solutions	
A	Pe_L	R	$\bar{\delta} \times 10^6$	$\delta_{\max} \times 10^6$	$\bar{\delta} \times 10^6$	$\delta_{\max} \times 10^6$	$\Delta \times 10^6$	$\Delta_{max} \times 10^6$
10	0.01	1	8.67	66.39	8.67	66.39	5.28×10^{-9}	2.31×10^{-2}
		$10^{0.5}$	9.33	74.47	9.33	14.47	3.15×10^{-3}	45.7
		10	11.69	94.12	11.69	94.12	3.87	3287.23
	0.1	1	8.67	66.45	8.67	66.45	5.11×10^{-9}	2.34×10^{-2}
		$10^{0.5}$	9.33	73.67	9.33	73.67	3.15×10^{-3}	45.78
		10	11.70	94.33	11.70	94.33	3.67	3287.27
	1	1	8.47	68.31	8.47	68.31	$5.24x10^{-9}$	3.76×10^{-2}
		$10^{0.5}$	9.01	74.23	90.14	74.23	2.06×10^{-3}	62.17
		10	11.29	94.61	11.29	94.61	3.39	4102.87

Table 5.2: Mean and maximum absolute percentage errors for series solutions and the difference between the solutions for a fixed value of Pe_B.

Parameters			Finite domain solution		Semi-infinite domain solutions		Absolute difference between solutions	
A	Pe_B	R	$\bar{\delta} \times 10^6$	$\delta_{\max} \times 10^6$	$\bar{\delta} \times 10^6$	$\delta_{\max} \times 10^6$	$\Delta \times 10^6$	$\Delta_{max} \times 10^6$
10	0.01	1	0.713	67.9	0.71	67.9	5.63×10^{-9}	1.12×10^{-1}
		$10^{0.5}$	0.827	76.7	0.827	76.7	3.13×10^{-3}	1127.13
		10	1.14	94.27	1.14	94.27	3.92	5380.27
	0.1	1	0.717	68.4	0.717	68.4	5.42×10^{-9}	1.58×10^{-1}
		$10^{0.5}$	0.823	75.5	0.823	75.5	2.91×10^{-3}	1222.43
		10	1.14	94.32	1.14	94.32	3.84	5373.39
	1	1	0.717	68.4	0.717	68.4	5.42×10^{-9}	0.158
		$10^{0.5}$	0.823	75.5	0.823	75.5	2.91×10^{-3}	1222.43
		10	1.14	94.32	1.14	94.32	3.84	5373.39

5.2 The effect of R in the dimensionless mean concentration profile

The impact of D_T on solute dispersion within the porous domain is illustrated in Figure 5.1 by the change of R for a given fixed value of Pe_L. It's worth noting that a higher R value corresponds to a larger Pe_L number, leading to greater dimensionless concentration values for a given ζ location, indicating a more dominant transport in the axial direction.

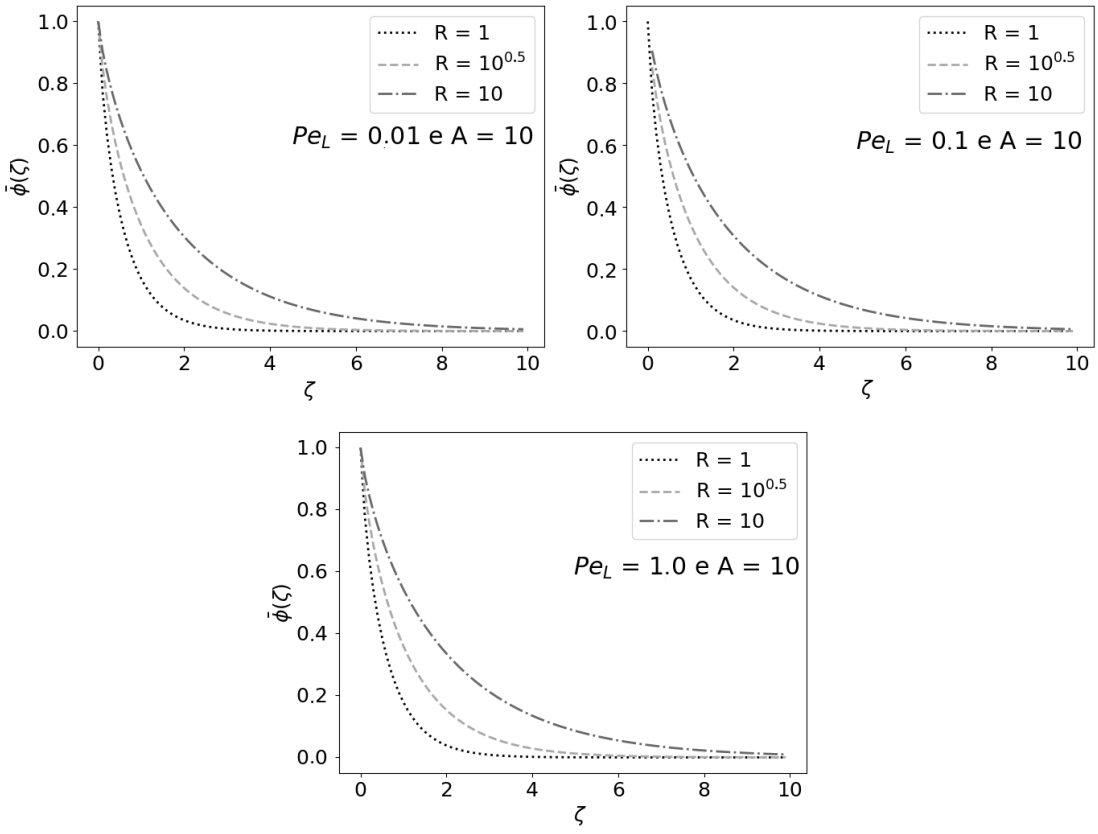

Figure 5.1: Influence of D_T via R (fixed Pe_L) in $\bar{\phi}(\zeta)$ profiles with $A = 10$.

An analogous evaluation is carried out to explore the responsiveness of $\bar{\phi}$ profiles to variations in D_L using R for fixed Pe_B and A, which is shown in Figure 5.2.

It should be noted that a value for Pe_B can be determined for a given D_T and A, which allows for the estimation of D_L using R. For $Pe_B = 0.01$ and $A = 10$, the values for Pe_L are 0.1, $10^{-1.5}$, and 0.01 for R equal to 1, $10^{0.5}$, and 10, respectively.

Similarly, for $Pe_B = 0.1$ and the same values of R, Pe_L values are 1, $10^{-0.5}$, and 0.1, respectively. The criterion $\delta_{\max}(\zeta_i) < 10^{-4}$ was imposed in determining the values of $\bar{\phi}$ at each point using both analytical solutions. Figure 5.2 demonstrates the sensitivity of $\bar{\phi}$ profiles to changes in the D_L values.

$$R = \frac{D_L}{D_T}\frac{vL}{vL} = \frac{\frac{vB}{D_T}}{\frac{vL}{D_L}} = \frac{L}{B} = \frac{Pe_B A}{R} \quad \rightarrow Pe_L = \frac{Pe_B A}{R} \tag{5.1}$$

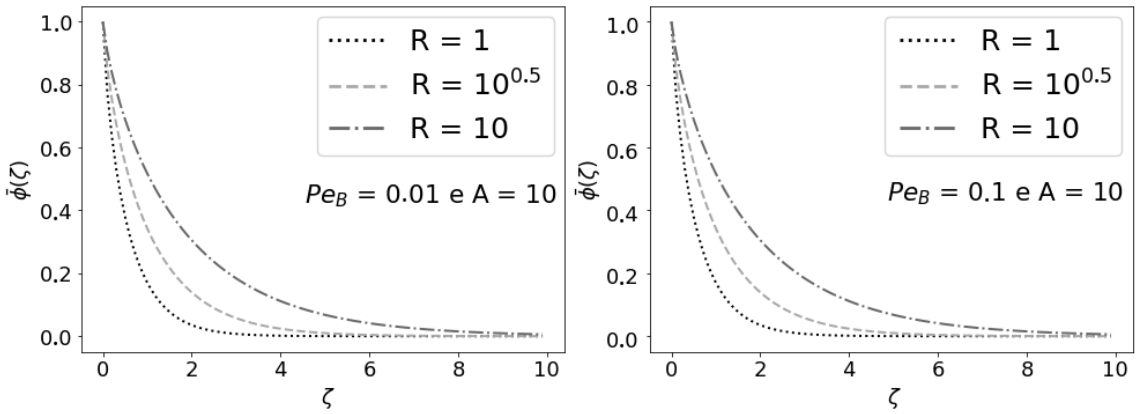

Figure 5.2: Influence of D_L via R (fixed Pe_B) in $\bar{\phi}$ profiles with $A = 10$ using the analytical solution for finite domain.

This analysis shows that $\bar{\phi}$ profiles are sensitive to changes in D_T and D_L, which means that $\bar{\phi}$ data can be used to estimate one or both dispersion coefficients.

5.3 Estimation of D_T using the SVA

The results in this section are related to the determination of the appropriate sub-volume thickness ($\mathcal{L}$) required to reliably estimate the value of R, the impact of the domain's length and height on the estimates of R and $\mathcal{D}_{vt}$, and the influence of different realisations on the $\mathcal{D}_{vt}$ value.

5.3.1 Sub-volume width analysis

To determine the required $\mathcal{L}$ value for estimating R, specific values were selected, specifically $1, 3, 5, 7, 9, 13$, and 21, and R values were estimated from the resulting

$\bar{\phi}$ profiles for Pe_m values of 1 and 10. The results showed that $\mathcal{L} \geqslant 5$ were needed for both Pe_m numbers, because the estimated R values independent of the $\mathcal{L}$ value. Table 5.3 list the networks and the corresponding R and $e_{95}(R)$ for $\zeta = 5, 7$ and 9. The values of sub-volume thickness and $\mathcal{D}_v \pm e_{95}(\mathcal{D}_v)$ were calculated using the SVA methodology, which the procedure can be found in the work of MACHADO *et al.* (2023).

Table 5.3: Values for R parameter with their respective 95% confidence error, $e_{95}(R)$, considering the whole domain length.

Pe_m	Network	$\mathcal{D}_v \pm e_{95}(\mathcal{D}_v)$	$R \pm e_{95}(R)$		
			$\zeta = 5$	$\zeta = 7$	$\zeta = 8$
1	C1	0.8595 ± 0.0024	1.3508 ± 0.0010	1.3508 ± 0.0010	1.3508 ± 0.0010
	C3	0.8590 ± 0.0009	1.3537 ± 0.0007	1.3537 ± 0.0007	1.3537 ± 0.0007
	C4	0.8591 ± 0.0015	1.3576 ± 0.0003	1.3576 ± 0.0003	1.3576 ± 0.0003
	CZ1	0.8506 ± 0.0021	1.8468 ± 0.0017	1.8468 ± 0.0017	1.8468 ± 0.0017
	CZ3	0.8367 ± 0.0029	1.8574 ± 0.0016	1.8574 ± 0.0016	1.8574 ± 0.0016
	CZ4	0.8204 ± 0.0014	1.8521 ± 0.0003	1.8521 ± 0.0003	1.8521 ± 0.0003
10	C3	8.1610 ± 0.0104	4.3333 ± 0.0023	4.3333 ± 0.0023	4.3333 ± 0.0023
	C4	8.1284 ± 0.0138	4.4066 ± 0.0017	4.4066 ± 0.0017	4.4066 ± 0.0017
	CZ3	9.9756 ± 0.0017	3.0767 ± 0.0015	3.0767 ± 0.0015	3.0767 ± 0.0015
	CZ4	9.8925 ± 0.0424	3.0894 ± 0.0005	3.0894 ± 0.0005	3.0894 ± 0.0005

For each network realisation and Pe_m value, Table 5.3 shows that the value of R vary within the error margins for different values of $\mathcal{L}$, indicating that the length of the sub-domain does not significantly influence the value of R. Table 5.3 also shows that the domain lengths can significantly impact the R value for the same network type, specially for $Pe_m = 10$. Therefore, it is crucial to investigate how domain length affects the R estimate.

Figure 5.3 shows the mean dimensionless concentration profile along the number of the pores layer in flow direction for different $\mathcal{L}$ values for the C1 pore network. In essence, upon initial inspection of these profiles, they appeared identical. Note

that plotting $\bar{\phi}$ using the number of layers, N_{Layers}, in cubic networks implies that there are approximately the same number of pores for given N_{Layer} value and type of network.

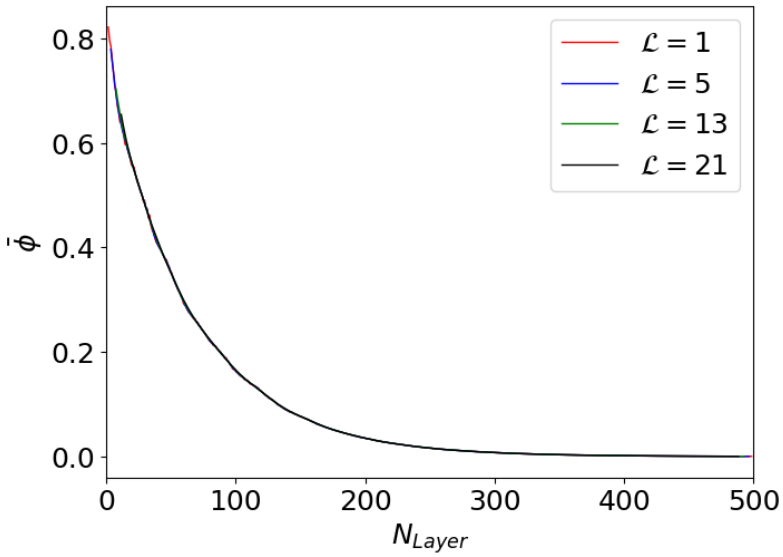

Figure 5.3: Dimensionless concentration profile along the pore layer number in flow direction for C1 network and $Pe_m = 1$.

To investigate the minor differences in the concentration profiles, a closer examination near the inlet was conducted. Figures 5.4 (a) and (b) display $\bar{\phi}$ for C3 and C4 networks, respectively. For $\mathcal{L} = 1$, there are results in oscillations in the $\bar{\phi}$ profiles, making this sub-volume thickness not suitable for estimating R. A comparison of the peak value of $e_{95}(\bar{\phi})$ in Figures 5.5 (a) and (b) with $\mathcal{L} = 1$ and 5, and then between $\mathcal{L} = 5$ and 21, reveals a reduction of about 50%. It is worth noting that this trend is observed in the results for all networks, either $Pe_m = 1$ or $Pe_m = 10$, as illustrated in Figures 5.6 and 5.7. As shown in Figure 5.7 the $e_{95}(\bar{\phi})$ profiles for $Pe_m = 10$ exhibit significantly more oscillations than those with $Pe_m = 1$.

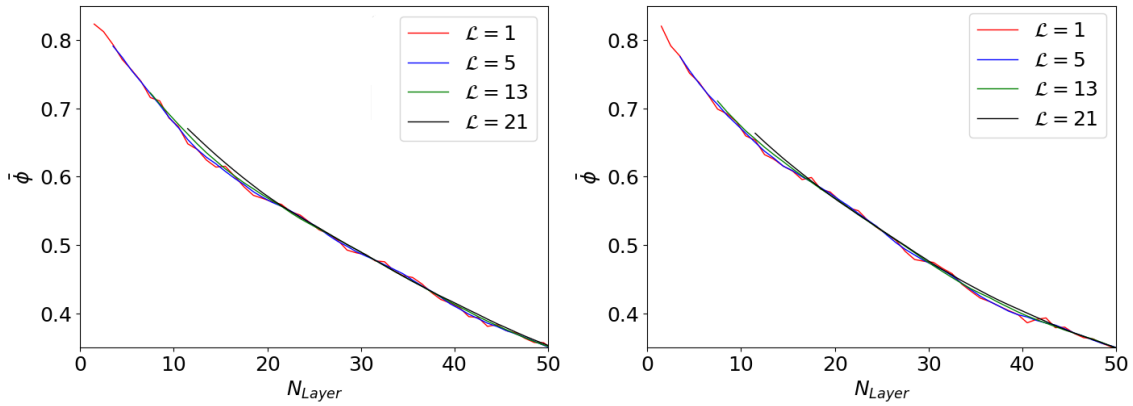

(a) (b)

Figure 5.4: Dimensionless concentration profiles near the inlet for different sub-volume thicknesses obtained with $Pe_m = 1$ for (a) C3 and (b) C4 networks.

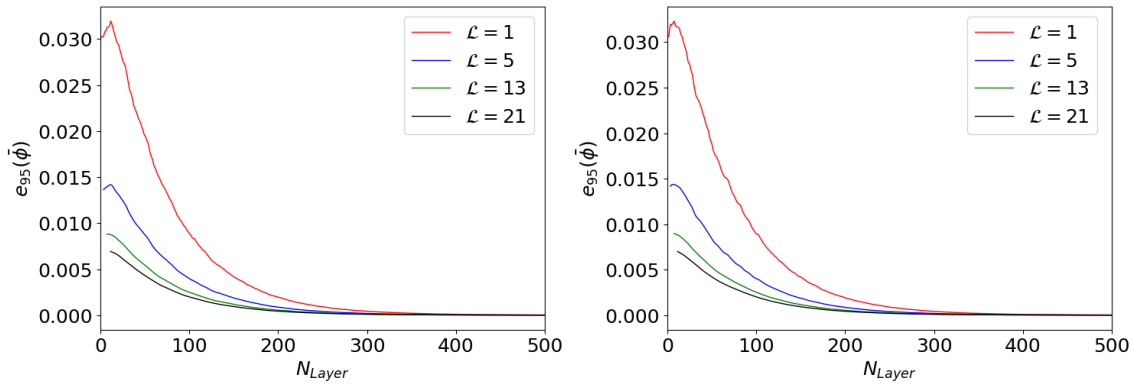

(a) (b)

Figure 5.5: $e_{95}(\bar{\phi})$ profiles along the domain in flow direction for different sub-volume thicknesses obtained with $Pe_m = 1$ for (a) C3 and (b) C4 networks.

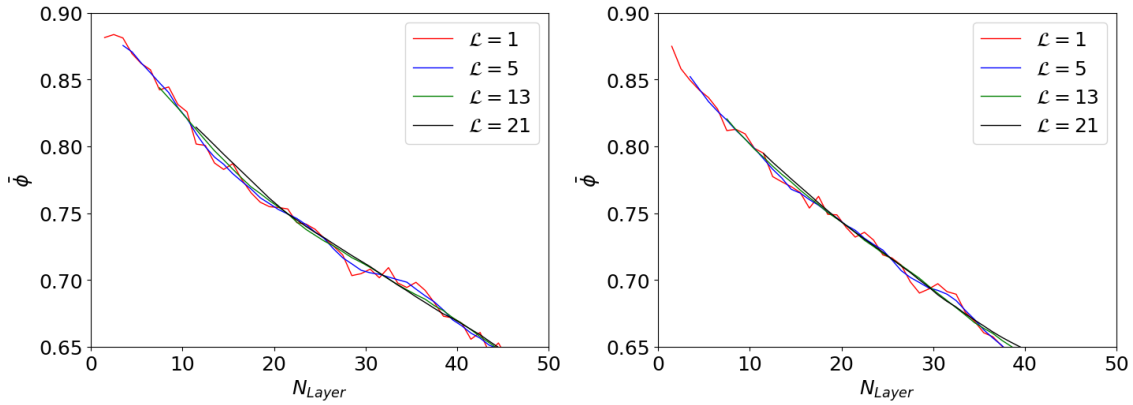

(a) (b)

Figure 5.6: Dimensionless concentration profiles near the inlet for different sub-volume thicknesses obtained with $Pe_m = 10$ for (a) C3 and (b) C4 networks.

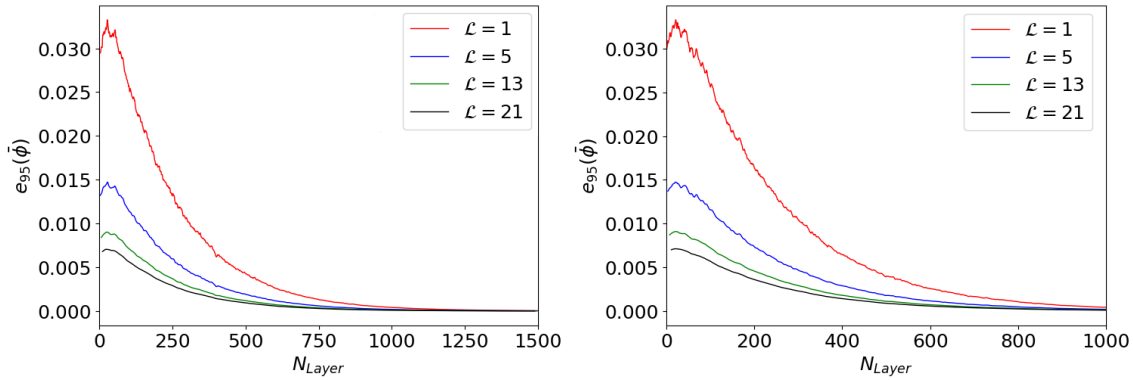

(a) (b)

Figure 5.7: $e_{95}(\bar{\phi})$ profiles along domain in flow direction for different sub-volume thicknesses obtained with $Pe_m = 10$ for (a) C3 and (b) C4 network.

5.3.2 Influence of domain length and height in estimating R

The variation in tracer concentration within the network is influenced by the porous and throat size heterogeneity and coordination number during mass transport. A higher concentration distribution in the transversal direction leads to a higher standard deviation. The dimensionless concentration varies from 1 at the inlet to zero at a sufficiently large ζ value. However, an excessively long pore network presents a large region with $\bar{\phi}$ close to zero where the standard deviation is quite small. Figures 5.8 (a) - (f) illustrate the dimensionless concentration profile for C and CZ network

types with $Pe_m = 1$. The band region represents the mean concentration standard deviation, with the highest value near the inlet that decreases to zero along the domain length. For $Pe_m = 1$, we observed that all networks are long enough to $\bar{\phi} \to 0$, and the longer the domain length, the greater the number of low values for $\sigma(\bar{\phi})$. This result directly impacts the estimation of $e_{95}(R)$ as we can see in Table 5.3, where the longer the length, the lower the R error, for the same type of pore network.

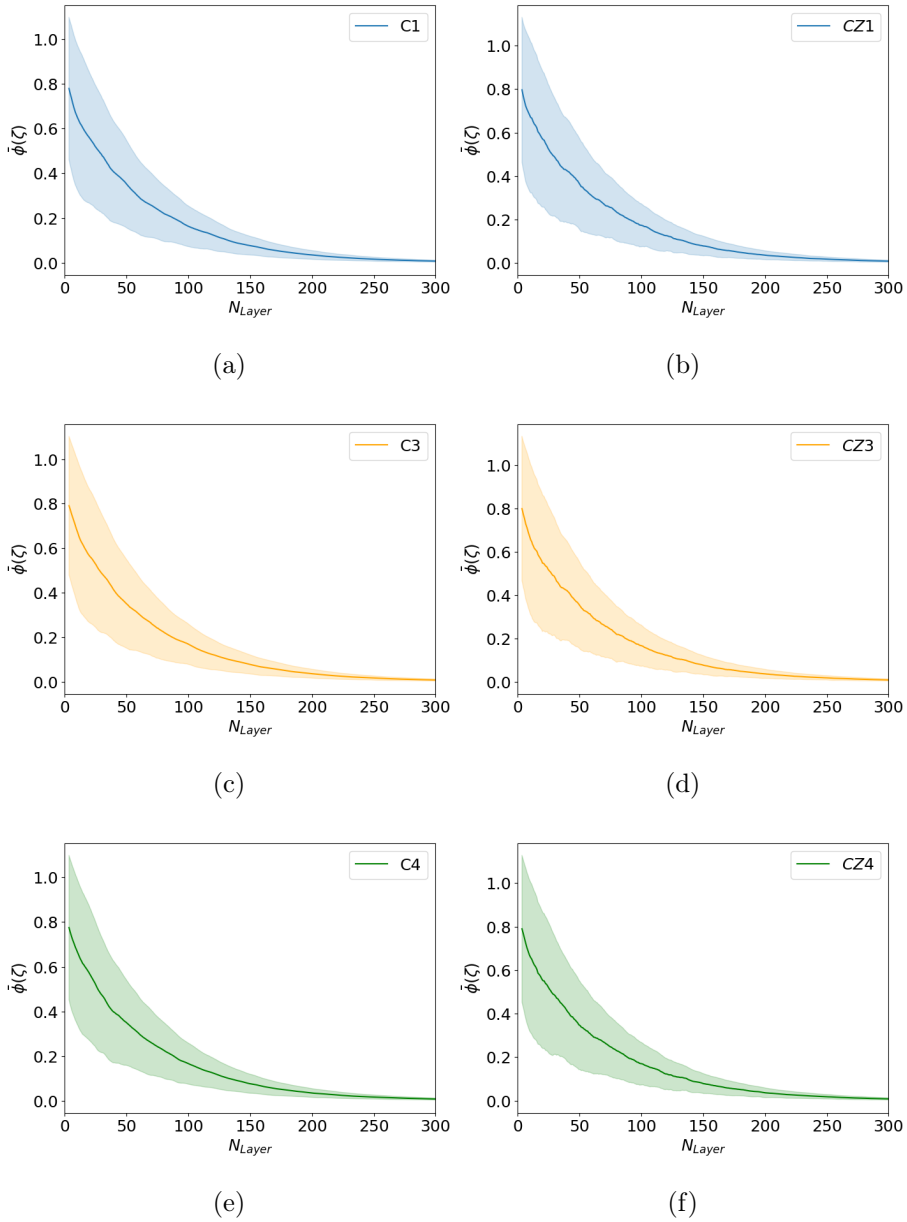

Figure 5.8: Dimensionless concentration profile along the pores' layer number in flow direction with bands which represent the $\sigma(\bar{\phi})$ for $Pe_m = 1$ with $\mathcal{L} = 5$ for C and CZ type network.

For $Pe_m = 1$, both network types achieved a near-zero $\bar{\phi}$ value at almost the same layer number. This is explained by the R values close to one (Table 5.3), which makes D_L and D_T approach D_m, for both network types. For this low value of Pe_m, diffusion transport is also important within the network elements.

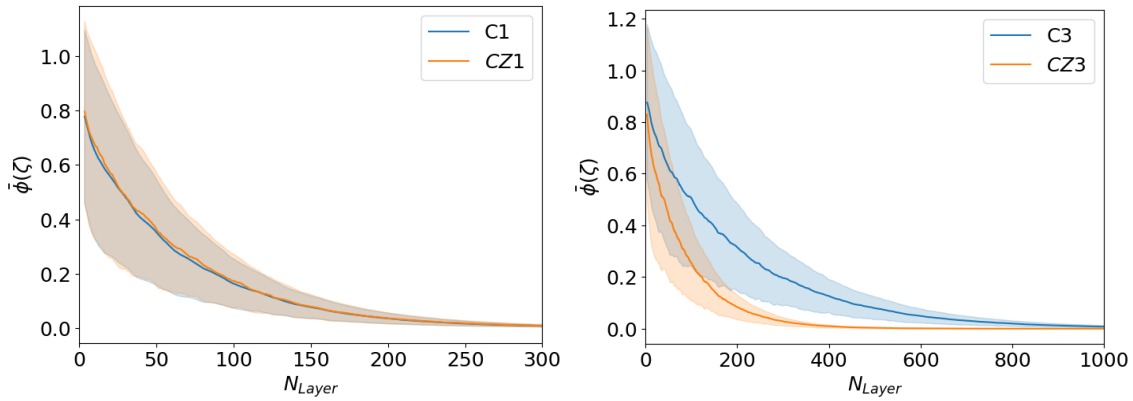

(a) (b)

Figure 5.9: Dimensionless concentration profile along the pores' layer number in flow direction with bands which represent $\sigma(\bar{\phi})$ with $\mathcal{L} = 5L$ for different types of network with (a) $Pe_m = 1$ and (b) $Pe_m = 10$.

In Figures 5.9 (a) and (b), compare $\bar{\phi} \pm \delta(\bar{\phi}$ for different network types simulated with $Pe_m = 1$ and 10, respectively. It can be observed that both network types reach $\bar{\phi} - 0$ at a similar position for $Pe_m = 1$. However, for $Pe_m = 10$, the $\bar{\phi}$ values drop to near zero at a lower N_{Layer} value for the CZ-type network when compared to the C-type network. This is explained by the smaller R values for the former networks shown in Table 5.3. The smaller R values determined for the CZ networks originate from their larger heterogeneity when compared to the C networks. This effect is pronounced for $Pe_m = 10$ because advection is dominant within the network elements.

To reduce $\sigma(\bar{\phi})$ values, two networks were modified by doubling their height (denoted as $2h$). This strategy increases the number of elements utilised to calculate the concentration standard deviation within a sub-volume, subsequently used to determine R and $e_{95}(R)$, which should be more accurate.

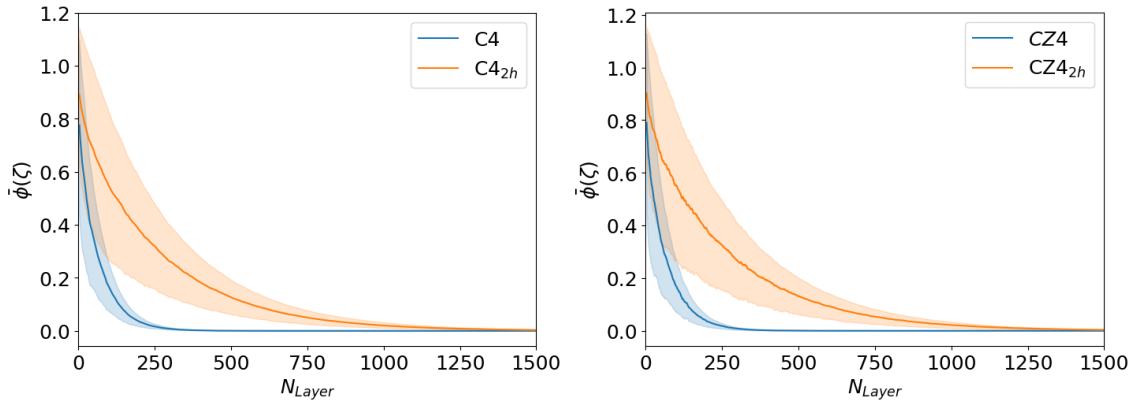

(a) (b)

Figure 5.10: Dimensionless concentration profile along the pores' layer number in flow direction with bands which represent $\sigma(\bar{\phi})$ with $\mathcal{L} = 5$ for $C4, C4_{2h}, CZ4$ and $CZ4_{2h}$ with $Pe_m = 1$.

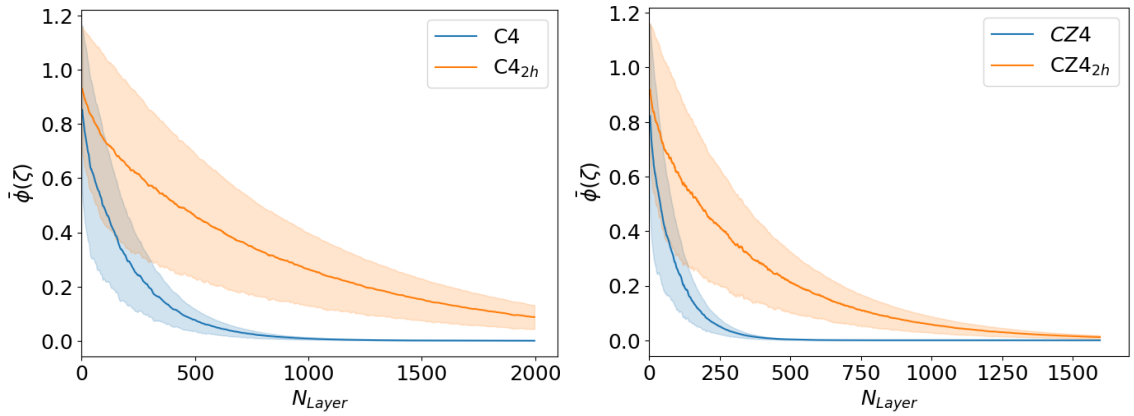

(a) (b)

Figure 5.11: Dimensionless concentration profile along the pores layer number in flow direction with bands which represent the mean concentration standard deviation with $\mathcal{L} = 5L_{pp}$ for $C4, C4_{2h}, CZ4$ and $CZ4_{2h}$ with $Pe_m = 10$.

Figure 5.10 (a) displays the $\bar{\phi}$ profiles for the C4 and $C4_{2h}$ networks realisations with $Pe_m = 1$ whereas 5.10 (b) shows the corresponding results for the CZ4 and $CZ4_{2h}$ networks. Figure 5.11 shows similar results, but, obtained with $Pe_m = 10$. It is evident that when the height is duplicated for the same Pe_m, the distance between the saturated boundaries increases. As a result, the solute must be transported over a longer longitudinal path to the $\bar{\phi}$ values become close to zero. As Pe_m increases, the value of N_{Layer} required to achieve $\bar{\phi} = 0$ increases as well. This is due to the fact

that advection becomes dominant, and the solute is transported faster in the flow direction. For instance, for C4 network, the fully developed mass transfer boundary layer is attained at $N_{Layer} \approx 250$ and 1000 for $Pe_m = 1$ and 10, respectively. Figure 5.11 shows that the $C4_{2h}$ pore network is not long enough to achieve the fully development region of the concentration boundary layer.

Figure 5.9 to 5.11 show that similarly to the case of Péclet number of 1, the $\delta(\bar{\phi})$ for all networks with $Pe_m = 10$ initially starts at a high value and decreases, reaching tiny values in the region where $\bar{\phi}$ is close to zero. Table 5.4 shows the used values of $\mathcal{D}_v \pm e_{95}(\mathcal{D}_v$ and the respective obtained values of R and its error for C4, $C4_{2h}$, CZ4 and $CZ4_{2h}$ networks for $Pe_m = 1$ and 10. The table reveals that doubling the domain's height resulted in a decrease in the $e_{95}(R)$ values, for $Pe_m = 1$. For $Pe_m = 10$ and the CZ4 networks, the opposite effect occurred.

Table 5.4: Values for R parameter with their respective 95% confidence error, $e_{95}(R)$, considering the whole domain length with $\mathcal{L} = 5$.

Pe_m	Network	$\mathcal{D}_v \pm e_{95}(\mathcal{D}_v)$	$R \pm e_{95}(R)$
1	C4	0.8591 ± 0.0015	1.3576 ± 0.0003
	$C4_{2h}$	0.8632 ± 0.0005	1.5381 ± 0.0002
	CZ4	0.8204 ± 0.0014	1.8521 ± 0.0003
	$CZ4_{2h}$	0.8256 ± 0.0021	2.0166 ± 0.0003
10	C4	8.1284 ± 0.0138	4.4066 ± 0.0017
	$C4_{2h}$	8.2142 ± 0.0151	4.5437 ± 0.0017
	CZ4	9.8925 ± 0.0424	3.0894 ± 0.0005
	$CZ4_{2h}$	9.8357 ± 0.0237	3.2808 ± 0.0009

Figure 5.12 (a) and (b) shows the profiles of $\sigma(\phi)/\bar{\phi}$ and $e_{95}\left(\bar{\phi}\right)/\bar{\phi}$, respectively, along the pores' layer number for $C4$, $C4_{2h}$, $CZ4$ and $CZ4_{2h}$ pore networks for $Pe_m = 10$ and sub-volume with 5 layers. Figure 5.12 (a), reveals that networks with the duplicated distance between boundary conditions exhibit slightly smaller values of $\sigma(\phi)/\bar{\phi}$, indicating that the smaller networks have already achieved a reasonable level of heterogeneity. Additionally, Figure 5.12 (b) illustrates the differences in

$e_{95}\left(\bar{\phi}\right)/\bar{\phi}$ achieved when the number of pores within a sub-volume is duplicated. When duplicating the height of a network the number of pores in the sub-volume is duplicated. Figure 5.12 shows that increasing the pore number for the same sub-volume thickness did not significantly change the concentration standard deviation or the 95% confidence error.

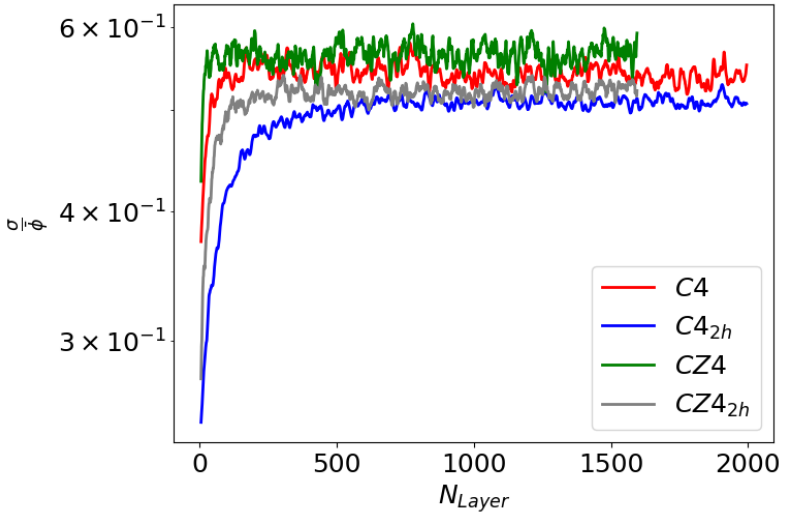

(a)

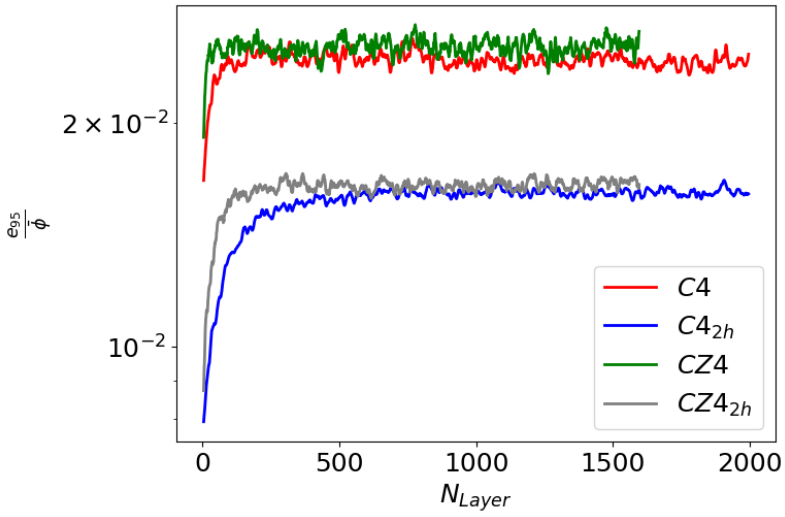

(b)

Figure 5.12: Profile of $\sigma(\phi)/\bar{\phi}$ (a) and $e_{95}\left(\bar{\phi}\right)/\bar{\phi}$ (b) throughout the pores layer number for C4, $C4_{2h}$, CZ4 and $CZ4_{2h}$ pore networks for $Pe_m = 10$ and sub-volume with 5 layers.

Despite using high values of $\sigma(\bar{\phi})$ to estimate R and its 95% confidence error, the latter remained low. This was shown to be due to the large number of $\bar{\phi}$ and $\delta(\bar{\phi})$

data close to zero that were used in the parameter estimation process. As previously mentioned, simulations with $Pe_m = 1$ quickly attain the value of $\bar{\phi} = 0$, but there is a long "tail" with a substantial amount of $\bar{\phi}$ and $\sigma(\bar{\phi})$ data that was used. This potentially masks the actual value of $e_{95}(R)$.

5.3.3 The data selection criterion for estimating R

Accurately calculating $e_{95}(R)$ is crucial since it is utilised to estimate $e_{95}(\mathcal{D}_{vt})$. Once the concentration data and associated errors from pore network simulation are gathered, the estimation process for R and $\mathcal{D}_{vt}$ can commence. However, it was discovered that even for high values of $\sigma(\bar{\phi})$, the values of $e_{95}(R)$ remained low when all the $\bar{\phi}$ data were employed to determine R. This was due to the numerous points near $\bar{\phi} = 0$ with very low values of $\sigma(\bar{\phi})$ incorporated into the estimation of R.

The criterion for data selection described in section 4 allowed for the estimation of new values for R and $\mathcal{D}_{vt}$ as shown in Table 5.5.

Table 5.5: Values for R parameter with its respective 95% confidence error, $e_{95}(R)$, considering the whole domain length and using the data selection criterion with $\bar{\phi}_{min} = 0.02$. The sub-volume width is $5L_{pp}$.

Pe_m	Network	$\zeta \in [0, A]$		$\zeta \in [0, \zeta_{max}]$	
		$R \pm e_{95}(R)$	A	$R \pm e_{95}(R)$	ζ_{max}
1	C1	1.3508 ± 0.0010	50	1.3371 ± 0.0033	23.55
	C3	1.3537 ± 0.0007	150	1.3661 ± 0.0027	23.55
	C4	1.3576 ± 0.0003	200	1.3296 ± 0.0030	23.55
	$C4_{2h}$	1.5381 ± 0.0002	200	1.4388 ± 0.0006	50.17
	CZ1	1.8468 ± 0.0017	40	1.8785 ± 0.0028	23.85
	CZ3	1.8574 ± 0.0016	40	1.8357 ± 0.0022	23.98
	CZ4	1.8521 ± 0.0003	160	1.8458 ± 0.0044	24.35
	$CZ4_{2h}$	2.0166 ± 0.0003	160	1.9851 ± 0.0010	51.32
10	C3	4.3333 ± 0.0023	150	4.2976 ± 0.0044	79.25
	C4	4.4066 ± 0.0017	200	4.2466 ± 0.0044	79.25
	$C4_{2h}$	4.5437 ± 0.0017	100	4.5433 ± 0.0017	99.9
	CZ3	3.0767 ± 0.0015	120	3.0357 ± 0.0061	29.65
	CZ4	3.0894 ± 0.0005	160	3.0436 ± 0.0047	29.65
	$CZ4_{2h}$	3.2808 ± 0.0009	80	3.2295 ± 0.0024	69.67

The findings in Table 5.5 align with the observations made in the previous section. Networks with the same type and for each Pe_m have the same development of the concentration boundary layer. For example, for $Pe_m = 1$, $C1$, $C3$, and $C4$ all have the same ζ_{max}, and the same pattern can be seen in $CZ1, CZ3$, and $CZ4$ networks. When the data selection criterion is activated, the required domain length to estimate R decreases significantly for all networks with $Pe_m = 1$. However, because many points near $\bar{\phi} = 0$ are no longer used, the $e_{95}(R)$ increases. As the Péclet number increases, the ζ_{max} value also increases for the same type of network. This is due to the increased advective solute transport in the longitudinal direction, with $\bar{\phi}$ taking longer to achieve zero. It is worth noting that for $C4_{2h}$ with $Pe_m = 10$,

the domain length required remains the same, as the fully developed mass transfer boundary layer is not achieved, since $\zeta_{max} \approx A - (\mathcal{L} - 1)\frac{L_{pp}}{L_y}$.

Table 5.6: Dimensionless longitudinal dispersion coefficient values, D_v, and transverse, D_{vt}, with their 95% confidence error. The latter is obtained using domain length truncated by the data selection criterion with $\bar{\phi}_{min} = 0.02$. The sub-volume width is $5L_{pp}$.

Pe_m	Network	$\mathcal{D}_v \pm e_{95}(\mathcal{D}_v)$	$R \pm e_{95}(R)$		
			$\zeta = 5$	$\zeta = 7$	$\zeta = 8$
1	C1	0.8595 ± 0.0024	0.6428 ± 0.0024	0.6428 ± 0.0024	0.6428 ± 0.0024
	C3	0.8590 ± 0.0009	0.6288 ± 0.0015	0.6288 ± 0.0015	0.6288 ± 0.0015
	C4	0.8591 ± 0.0015	0.6461 ± 0.0018	0.6461 ± 0.0018	0.6461 ± 0.0018
	$C4_{2h}$	0.8632 ± 0.0005	0.5999 ± 0.0004	0.5999 ± 0.0004	0.5999 ± 0.0004
	CZ1	0.8506 ± 0.0021	0.4528 ± 0.0013	0.4528 ± 0.0013	0.4528 ± 0.0013
	CZ3	0.8367 ± 0.0029	0.4514 ± 0.0017	0.4514 ± 0.0017	0.4514 ± 0.0017
	CZ4	0.8204 ± 0.0014	0.4445 ± 0.0013	0.4445 ± 0.0013	0.4445 ± 0.0013
	$CZ4_{2h}$	0.8256 ± 0.0021	0.4159 ± 0.0011	0.4159 ± 0.0011	0.4159 ± 0.0011
10	C3	8.1610 ± 0.0104	1.8990 ± 0.0031	1.8990 ± 0.0031	1.8990 ± 0.0031
	C4	8.1284 ± 0.0138	1.9141 ± 0.0038	1.9141 ± 0.0038	1.9141 ± 0.0038
	$C4_{2h}$	8.2142 ± 0.0151	1.8080 ± 0.0112	1.8080 ± 0.0112	1.8080 ± 0.0112
	CZ3	9.9756 ± 0.0017	3.2861 ± 0.0066	3.2861 ± 0.0066	3.2861 ± 0.0066
	CZ4	9.8925 ± 0.0424	3.2503 ± 0.0148	3.2503 ± 0.0148	3.2503 ± 0.0148
	$CZ4_{2h}$	9.8357 ± 0.0237	3.0456 ± 0.0077	3.0456 ± 0.0077	3.0456 ± 0.0077

Table 5.6 lists the $\mathcal{D}_v$ and $\mathcal{D}_{vt}$ values for all network realisations previously analysed for $Pe_m = 1$ and 10 for different values of sub-volume thickness. Immediately one can realise that when $\mathcal{L} \geq 5$, the values of $R \pm e_{95}(R)$ are equal, meaning that $\mathcal{L} = 5$ is the sub-volume thickness that can be used for the analysis. It also reveals that the length and height of the domain do not account for the excess of low values of $\sigma(\bar{\phi})$. For $Pe_m = 1$, the values of $\mathcal{D}_v$ for the same network type agree within their error margins, indicating that length does not significantly affect the determination of $\mathcal{D}_v$ for this flow regime, for which that the solute transport by diffusion

is important. For the solute transport in the transverse direction, the possible flow paths from one pore to another are crucial. As the CZ networks have a distribution of pore connectivities, the values of $\mathcal{D}_{vt}$ for the CZ networks are about 30% smaller than those for the C networks.

For $Pe_m = 10$, the $\mathcal{D}_v$ values of the C3 and C4 realisations agree within their error margins and those for CZ3 and CZ4 only agree within twice their error margins. The $\mathcal{D}_v$ results for C4 and $C4_{2h}$ networks and for CZ4 and $CZ4_{2h}$ networks differs 1%. However, these differences are about 2-3 times the sum of the estimated uncertainties. The estimated values of $\mathcal{D}_{vt}$ for the C4 and $C4_{2h}$ and for CZ4 and $CZ4_{2h}$ differ by $5-6\%$, indicating a more crucial role played by boundary conditions in determining the transverse dispersion coefficient.

Table 5.6 also highlights the importance of achieving the fully developed transfer mass boundary layer for estimating $e_{95}(\mathcal{D}_{vt})$, once this condition is not achieved as in the case of $C4_{2h}$, the increase in the number of pores in the sub-volume does not decrease the error for both dispersion coefficient. It is worth noting that both $CZ4$ and $CZ4_{2h}$ achieve this condition, resulting in a reduction of almost 50% in $e_{95}(\mathcal{D}_{vt})$. The significance of achieving the fully developed boundary layer is evident in the simulations with $Pe_m = 10$ and network $C4_{2h}$. Interestingly, duplicating the number of pores inside a sub-volume did not decrease the value of $e_{95}(\mathcal{D}_{vt})$ but instead increased it.

To verify the effect of the estimation error of $\mathcal{D}_v$ in the results for $\mathcal{D}_{vt}$, new values of the dimensionless transverse dispersion coefficient are calculated using the perturbed $\mathcal{D}_v$ values given by:

$$\mathcal{D}_v^+ = \mathcal{D}_v + e_{95}(\mathcal{D}_v) \tag{5.2}$$

$$\mathcal{D}_v^- = \mathcal{D}_v - e_{95}(\mathcal{D}_v) \tag{5.3}$$

Using $\mathcal{D}_v^+$ and $\mathcal{D}_v^-$ to estimate R and $e_{95}(R)$, and, therefore new values for the

dimensionless transverse coefficients $\mathcal{D}_{vt}^{+}$ and $\mathcal{D}_{vt}^{-}$. The 95% confidence error was calculated as detailed in equation 4.8, with the value of $e_{95}(\mathcal{D}_v)$ remaining the same as presented in Table 5.6.

Table 5.7: $\mathcal{D}_{vt}^{+}$ and $\mathcal{D}_{vt}^{-}$, with their 95% confidence error, using the domain truncated by the data selection criterion with $\bar{\phi}_{min} = 0.02$. The sub-volume width is $5L_{pp}$.

Pe_m	Network	$\mathcal{D}_{vt}^{+} \pm e_{95}(\mathcal{D}_{vt}^{+})$	$\mathcal{D}_{vt}^{-} \pm e_{95}(\mathcal{D}_{vt}^{-})$
1	$C1$	0.6428 ± 0.0027	0.6427 ± 0.0021
	$C3$	0.6289 ± 0.0016	0.6288 ± 0.0013
	$C4$	0.6461 ± 0.0018	0.6461 ± 0.0014
	$C4_{2h}$	0.5999 ± 0.0006	0.5999 ± 0.0004
	$CZ1$	0.4528 ± 0.0014	0.4528 ± 0.0011
	$CZ3$	0.4518 ± 0.0017	0.4510 ± 0.0016
	$CZ4$	0.4500 ± 0.0032	0.4500 ± 0.0029
	$CZ4_{2h}$	0.4295 ± 0.0012	0.4295 ± 0.0010
10	$C3$	1.8990 ± 0.0035	1.8990 ± 0.0028
	$C4$	1.9141 ± 0.0040	1.9141 ± 0.0035
	$C4_{2h}$	1.8080 ± 0.0118	1.8079 ± 0.0107
	$CZ3$	3.2861 ± 0.0068	3.2860 ± 0.0066
	$CZ4$	3.2371 ± 0.0149	3.2371 ± 0.0147
	$CZ4_{2h}$	3.0456 ± 0.0078	3.0456 ± 0.0072

Comparing the values of $\mathcal{D}_{vt}^{+}$ and $\mathcal{D}_{vt}^{-}$ in Table 5.7 and $\mathcal{D}_{vt}$ in Table 5.6, it is possible to realise the dimensionless transverse dispersion coefficient is not sensitive to the values of the dimensionless longitudinal dispersion coefficient within its error margin.

5.3.4 The effect of different network realisations in determining D_T

Despite the network of the same type being equal statically, the spatial distribution of pore and throat sizes for the C-type networks and also the spatial distribution of pores and throats for the CZ-type networks are slightly different for each realisation. Thus, it is essential to understand how this can influence the determination of $\mathcal{D}_{vt}$.

Table 5.8 and 5.9 shows the $\mathcal{D}_{vt}$ value for ten realisations of the C4 and CZ4 networks with $Pe_m = 1$ and 10, respectively, using the data selection criterion with $\bar{\phi}_{min} = 0.02$. The values of the dimensionless transverse dispersion coefficient, $\langle \mathcal{D}_{vt} \rangle$, and its 95% confidence error, $e_{95}(\langle \mathcal{D}_{vt} \rangle)$ is presented for each realisation. Then, by adjusting a constant using the $\mathcal{D}_{vt} \pm e_{95}(\mathcal{D}_{vt})$ values for each realisation, it is also obtained the values for $\bar{\mathcal{D}}_{vt}$ and its 95% confidence error, $e_{95}(\bar{\mathcal{D}}_{vt})$. These tables show the values of $\langle \mathcal{D}_{vt} \rangle \pm e_{95}(\langle \mathcal{D}_{vt} \rangle)$ and $\bar{\mathcal{D}}_{vt} \pm e_{95}(\bar{\mathcal{D}}_{vt})$ agree within their error margins. Most of the values of $\mathcal{D}_{vt}$ for different realisations also agree within their error margins.

Table 5.8: Effect of network realisation in the determination of $\mathcal{D}_{vt}$ for C4 networks with $Pe_m = 1$ and 10 with the data selection criterion with $\bar{\phi}_{min} = 0.02$. R-numbers denote different realisations.

Pe_m	1	10
Realisation	$\mathcal{D}_{vt} \pm e_{95}(\mathcal{D}_{vt})$	
C4 - R01	0.6461 ± 0.0018	1.9142 ± 0.0038
C4 - R02	0.6466 ± 0.0017	1.9101 ± 0.0023
C4 - R03	0.6456 ± 0.0017	1.9204 ± 0.0025
C4 - R04	0.6482 ± 0.0015	1.9099 ± 0.0025
C4 - R05	0.6532 ± 0.0016	1.9178 ± 0.0029
C4 - R06	0.6493 ± 0.0015	1.9157 ± 0.0031
C4 - R07	0.6419 ± 0.0018	1.9144 ± 0.0038
C4 - R08	0.6448 ± 0.0018	1.9189 ± 0.0030
C4 - R09	0.6483 ± 0.0014	1.9201 ± 0.0029
C4 - R10	0.6433 ± 0.0015	1.9168 ± 0.0034
$\langle \mathcal{D}_{vt} \rangle \pm e_{95}(\langle \mathcal{D}_{vt} \rangle)$	0.6467 ± 0.0017	1.9213 ± 0.0038
$\bar{\mathcal{D}}_{vt} \pm e_{95}(\bar{\mathcal{D}}_{vt})$	0.6471 ± 0.0078	1.9226 ± 0.0042

Table 5.8 and 5.9 shows that $e_{95}(\langle \mathcal{D}_{vt} \rangle$ and $e_{95}(\bar{\mathcal{D}}_{vt})$ are almost identical when $Pe_m = 10$, but they differs by almost five times for $Pe_m = 1$. These tables also reveal that for $C4$ when $Pe_m = 1$ and 10, 70% and 80% of the $\mathcal{D}_{vt}$ values are in agreement with $\langle \mathcal{D}_{vt} \rangle$, respectively. On the other hand, for $CZ4$ these percentage drops to 60% and 40% when $Pe_m = 1$ and 10, respectively. This shows that for $C4$ and $CZ4$, the realisation of more than 1 realisation is required in order to obtain a mean value of the dimensionless transverse dispersion coefficient. The table 5.10 shows the mean and maximum value for the absolute difference between $\mathcal{D}_{vt,i}$ and $\mathcal{D}_{vt,j}$, $\overline{\Delta \mathcal{D}_{vt}}^{a}$ and $\Delta \mathcal{D}_{vt,max}$, respectively, and the mean and maximum value of the sum of their errors, $\overline{\Delta e_{95}}^{a}$ and $\Delta e_{95,max}$, respectively.

Table 5.9: Effect of network realisation in the determination of $\mathcal{D}_{vt}$ for CZ4 networks with $Pe_m = 1$ and 10 with the data selection criterion $\bar{\phi}_{min} = 0.02$. R-numbers denote different realisations.

Pe_m	1	10
Realisation	$\mathcal{D}_{vt} \pm e_{95}(\mathcal{D}_{vt})$	
CZ4 - R01	0.4445 ± 0.0013	3.2503 ± 0.0148
CZ4 - R02	0.4495 ± 0.0016	3.2797 ± 0.0062
CZ4 - R03	0.4528 ± 0.0012	3.3445 ± 0.0092
CZ4 - R04	0.4531 ± 0.0026	3.3400 ± 0.0066
CZ4 - R05	0.4464 ± 0.0015	3.2933 ± 0.0115
CZ4 - R06	0.4511 ± 0.0015	3.2992 ± 0.0137
CZ4 - R07	0.4449 ± 0.0015	3.2532 ± 0.0082
CZ4 - R08	0.4489 ± 0.0015	3.3219 ± 0.0128
CZ4 - R09	0.4548 ± 0.0015	3.3443 ± 0.0119
CZ4 - R10	0.4479 ± 0.0011	3.2964 ± 0.0090
$\langle\mathcal{D}_{vt}\rangle \pm e_{95}(\langle\mathcal{D}_{vt}\rangle)$	0.4494 ± 0.0015	3.3023 ± 0.0104
$\bar{\mathcal{D}}_{vt} \pm e_{95}(\bar{\mathcal{D}}_{vt})$	0.4501 ± 0.0027	3.3089 ± 0.0484

Table 5.10: Mean and maximum value of the difference between $\mathcal{D}_{vt,i}$ and $\mathcal{D}_{vt,j}$ and the sum of their errors for C4 and CZ4 networks with $Pe_m = 1$ and 10 with the data selection criterion $\bar{\phi}_{min} = 0.02$

Pe_m	Network	$\overline{\Delta\mathcal{D}_{vt}}^a$	$\Delta\mathcal{D}_{vt,max}$	$\overline{\Delta e_{95}}^a$	$\Delta e_{95,max}$
1	C4	0.0024	0.0065	0.0033	0.0035
	CZ4	0.0029	0.0054	0.0030	0.0041
10	C4	0.0055	0.0114	0.0057	0.0076
	CZ4	0.0283	0.0520	0.0208	0.0252

Chapter 6

Conclusions

In this study, we introduce the application of the sub-volume analysis (SVA) proposed by MACHADO *et al.* (2023), for determining the transverse dispersion coefficient from pore-network simulations. For statistically build pore networks, our approach involves calculating $\mathcal{D}_v$ using the SVA methodology, followed by determining $\mathcal{D}_{vt}$ using the techniques developed in this research. The findings also demonstrate that in order to estimate R and its 95% confidence error, sub-volumes with five layers of pores is suffice, as the values of R and its error no longer depends on the sub-volume thickness.

In addition, the study revealed that the length and height of the domain have an impact on the analysis. The $e_{95}(R)$ is sensitive to the data with near zero standard deviation, and the data selection criterion was developed to avoid masking the true value of $e_{95}(R)$. Furthermore, for $Pe_m = 10$, the transverse dispersion coefficient $\mathcal{D}_{vt}$ varies between 5%-6% as a result of increasing the domain's height highlighting the role of the boundary conditions. Also one realisation of the C4 or CZ4 networks can estimate $\mathcal{D}_{vt}$ of its error if assumed to be 2-5 times larger than $e_{95}(\mathcal{D}_{vt})$.

The findings indicate that the $(\langle \mathcal{D}_{vt} \rangle)$ and $\bar{\mathcal{D}}_{vt}$ values are in agreement within their error margins for the analysed network type. Unfortunately, this methodology is unable to determine both dispersion coefficients simultaneously due to the high correlation between $\mathcal{D}_v$ and $\mathcal{D}_{vt}$.

6.1 Future Work Suggestions

Based on the findings of this study, further research is required to gain a deeper understanding of how boundary conditions impact the calculation of $\mathcal{D}_{vt}$. Additionally, the analytical solutions put forth offer both dispersion coefficients, providing an opportunity to explore innovative approaches for simultaneous determination. Furthermore, the developed methodology can be tested using tomographically reconstructed pore networks to determine their transverse dispersion coefficient.

References

ACHARYA, R. C., VAN DER ZEE, S. E. A. T. M., LEIJNSE, A., 2007, "Approaches for modelling longitudinal dispersion in pore-networks", *Advances in water resources*, v. 30, n. 2, pp. 261–272.

ARIS, R., 1956, "On the dispersion of a solute in a fluid flowing through a tube", *Proceedings of the Royal Society of London. Series A. Mathematical and Physical Sciences*, v. 235, n. 1200, pp. 67–77.

ARIS, R., 1959, "On the dispersion of a solute by diffusion, convection and exchange between phases", *Proceedings of the Royal Society of London. Series A. Mathematical and Physical Sciences*, v. 252, n. 1271, pp. 538–550.

BABAEI, M., JOEKAR-NIASAR, V., 2016, "A transport phase diagram for pore-level correlated porous media", *Advances in Water Resources*, v. 92, pp. 23–29.

BAETSLE, L. H., 1969, "Migration of radionuclides in porous media", *Progress in Nuclear Energy, Series XII, Health Physics*, pp. 707–730.

BARON, T., 1952, "Generalized graphical method for the design of fixed bed catalytic reactors", *Chem. Eng. Prog*, v. 48, pp. 118.

BATTIATO, I., FERRERO V., P. T., O'MALLEY, D., et al., 2019, "Theory and applications of macroscale models in porous media", *Transport in Porous Media*, v. 130, pp. 5–76.

BEAR, J., 1988, *Dynamics of Fluids in Porous Media*. USAD, ARS, Baton Rouge, Louisiana, Dover.

BERG, M., DAVIT, Y., QUINTARD, M., et al., 2020, "Modelling solute transport in the brain microcirculation: is it really well mixed inside the blood vessels?" *Journal of Fluid Mechanics*, v. 884, pp. A39.

BERNARD, R. A., WILHELM, R. H., 1950, "urbulent diffusion in fixed beds of packed solids", *Ind. Eng. Chem.*, v. 46, n. 1, pp. 233.

BIJELJIC, B., BLUNT, M. J., 2007, "Pore-scale modeling of transverse dispersion in porous media", *Water Resources Research*, v. 43, n. 12.

BIJELJIC, B., MUGGERIDGE, A. H., BLUNT, M. J., 2004, "Pore-scale modeling of longitudinal dispersion", *Water resources research*, v. 40, n. 11.

BLUNT, M. J., BIJELJIC, B., DONG, H., et al., 2013, "Pore-scale imaging and modelling", *Advances in Water Resources*, v. 51, pp. 197–216. ISSN: 0309-1708. doi: https://doi.org/10.1016/j.advwatres.2012.03.003. Disponível em: <https://www.sciencedirect.com/science/article/pii/S0309170812000528>. 35th Year Anniversary Issue.

BRENNER, H., 1980, "Dispersion resulting from flow through spatially periodic porous media", *Philosophical Transactions of the Royal Society of London. Series A, Mathematical and Physical Sciences*, v. 297, n. 1430, pp. 81–133.

BRENNER, H., 1995, "The diffusion model of longitudinal mixing in beds of finite length. Numerical values", *Chemical Engineering Science*, v. 50, n. 24, pp. 3937–3947.

BRUDERER, C., BERNABÉ, Y., 2001, "Network modeling of dispersion: Transition from Taylor dispersion in homogeneous networks to mechanical dispersion in very heterogeneous ones", *Water resources research*, v. 37, n. 4, pp. 897–908.

CARBONELL, R. G., WHITAKER, S., 1983, "Dispersion in pulsed systems—II: theoretical developments for passive dispersion in porous media", *Chemical Engineering Science*, v. 38, n. 11, pp. 1795–1802.

CHAO, R., HOELSCHER, H. E., 1966, "Simultaneous axial dispersion and adsorption in a packed bed", *AIChE Journal*, v. 12, n. 2, pp. 271–278.

COELHO, M. A. N., DE CARVALHO, J. G., 1988, "Transverse dispersion in granular beds. I: Mass transfer from a wall and the dispersion coefficient in packed beds", *Chemical Engineering Research and Design*, v. 66, pp. 165–177. Disponível em: <https://api.semanticscholar.org/CorpusID:99353280>.

CRANK, J., 1979, *The Mathematics of Diffusion*. Oxford science publications. UK, Oxford, Clarendon Press. ISBN: 9780198534112. Disponível em: <https://books.google.co.uk/books?id=eHANhZwVouYC>.

DANCKWERTS, P. V., 1953, "Continuous flow systems Distribution of Residence times Chemical Engineering science genie chimique Vol. 2", *Chemical Engineering Science*.

DE CARVALHO, J. R. F. G., DELGADO, J. M. P. Q., 2000, "Lateral dispersion in liquid flow through packed beds at Pem< 1,400", *AIChE journal*, v. 46, n. 5, pp. 1089–1095.

DORWEILER, V. P., FAHIEN, R., 1959, "Mass transfer at low flow rates in a packed column", *AIChE Journal*, v. 5, n. 2, pp. 139–144.

EDWARDS, M. F., RICHARDSON, J. F., 1968, "Gas dispersion in packed beds", *Chemical Engineering Science*, v. 23, n. 2, pp. 109–123.

EIDSATH, A., CARBONELL, R. G., WHITAKER, S., et al., 1983, "Dispersion in pulsed systems—III: comparison between theory and experiments for packed beds", *Chemical Engineering Science*, v. 38, n. 11, pp. 1803–1816.

EVANS, E. V., KENNEY, C. N., 1966, "Gaseous Dispersion in Laminar Flow Through a Circular Tube with Mass Transfer to a Retentive Layer", *Proceedings of the Royal Society of London. Series A, Mathematical and Physical Sciences*, v. 293, n. 1435, pp. 562–572. ISSN: 00804630. Disponível em: <http://www.jstor.org/stable/2415581>.

FAHIEN, R. W., SMITH, J. M., 1955, "MASS TRANSFER IN PACKED BEDS", *A.I.Ch.E. Journal*, v. 1 (3). doi: 10.1002/aic.690010104. Disponível em: <https://www.osti.gov/biblio/4380054>.

FERRARI, A., LUNATI, I., 2014, "Inertial effects during irreversible meniscus reconfiguration in angular pores", *Advances in Water Resources*, v. 74, pp. 1–13. ISSN: 0309-1708. doi: https://doi.org/10.1016/j.advwatres.2014.07.009. Disponível em: <https://www.sciencedirect.com/science/article/pii/S0309170814001493>.

GOLPARVAR, A., ZHOU, Y., WU, K., et al., 2018, "A comprehensive review of pore scale modeling methodologies for multiphase flow in porous media", *Advances in Geo-Energy Research*, v. 2, n. 4, pp. 418–440.

GOSTICK, J., AGHIGHI, M., HINEBAUGH, J., et al., 2016, "OpenPNM: a pore network modeling package", *Computing in Science and Engineering*, v. 18, n. 4, pp. 60–74.

GRAY, W. G., 1975, "A derivation of the equations for multi-phase transport", *Chemical Engineering Science*, v. 30, n. 2, pp. 229–233.

GUNN, D. J., 1969, "Dispersion in packed beds", *Trans. Inst. Chem. Engers.*, v. 47, pp. T–341.

HAAS, A., SROCKA, M., 2023, "PyPardiso", *GitHub repository https://github.com/haasad/PyPardisoProject*.

HARRIS, C. R., MILLMAN, K. J., VAN DER WALT, S. J., et al., 2020, "Array programming with NumPy", *Nature*, v. 585, n. 7825, pp. 357–362.

HIBY, J. W., 1962, "Longitudinal dispersion in single-phase liquid flow through ordered and random packings", *Interaction Between Fluid and Particles (London Institution of Chemical Engineers)*, pp. 312–325.

HIGBIE, R., 1935, "The rate of absorption of pure gas into a still liquid during short periods of exposure", *Trans. Am. Inst. Chem. Engrs.*, v. 31, pp. 365–389.

HUNT, B., 1978, "Dispersive sources in uniform ground-water flow", *Journal of the Hydraulics Division*, v. 104, n. 1, pp. 75–85.

KLINKENBERG, A., KRAJENBRINK, H. J., LAUWERIER, H. A., 1953, "Diffusion in a fluid moving at uniform velocity in a tube", *Industrial and Engineering Chemistry*, v. 45, n. 6, pp. 1202–1208.

KLINKENBERG A., KRAJENBRINK H. J., L. H. A., 1953, "Diffusion in a fluid moving at uniform velocity in a tube", *Ind Eng Chem*, v. 45, pp. 118.

KOHNE, J. M., SCHLUTER, S., VOGEL, H.-J., 2011, "Predicting solute transport in structured soil using pore network models", *Vadose Zone Journal*, v. 10, n. 3, pp. 1082–1096.

KOU, J., WANG, X., CHEN, H., et al., 2023, "An efficient bound-preserving and energy stable algorithm for compressible gas flow in porous media", *Journal of Computational Physics*, v. 473, pp. 111751. ISSN: 0021-9991. doi: https://doi.org/10.1016/j.jcp.2022.111751. Disponível em: <https://www.sciencedirect.com/science/article/pii/S0021999122008142>.

KRAMERS, H., ALBERDA, G., 1953, "Frequency response analysis of continuous flow systems", *Chemical Engineering Science*, v. 2, n. 4, pp. 173–181.

LATINEN, G. A., 1951, "Mechanism of fluid-phase mixing in fixed and fluidised beds of uniformly sized spherical particles", *PhD thesis*.

LEVENSPIEL, O., SMITH, W. K., 1957, "Notes on the diffusion-type model for the longitudinal mixing of fluids in flow", *Chemical Engineering Science*, v. 6, n. 4-5, pp. 227–235.

LIU, Y., GONG, W., ZHAO, Y., et al., 2022, "A Pore-Throat Segmentation Method Based on Local Hydraulic Resistance Equivalence for Pore-Network Modeling", *Water Resources Research*, v. 58, n. 12, pp. e2022WR033142.

MACHADO, A. V. L., LAGE, P. L. C., COUTO, P., 2023, "Sub-volume analysis of pore-network simulations: Determining the asymptotic longitudinal dispersion coefficient", *Advances in Water Resources*, v. 181, pp. 104541. ISSN: 0309-1708. doi: https://doi.org/10.1016/j.advwatres.2023.104541. Disponível em: <https://www.sciencedirect.com/science/article/pii/S0309170823001756>.

MAIER, R. S., KROLL, D. M., BERNARD, R. S., et al., 2000, "Pore-scale simulation of dispersion", *Physics of Fluids*, v. 12, n. 8, pp. 2065–2079.

MCHENRY JR., K. W., WILHELM, R. H., 1957, "Axial mixing of binary gas mixtures flowing in a random bed of spheres", *AIChE Journal*, v. 3, n. 1, pp. 83–91.

MEHMANI, Y., XU, K., 2022a, "Pore-network modeling of Ostwald ripening in porous media: How do trapped bubbles equilibrate?" *Journal of Computational Physics*, v. 457, pp. 111041. ISSN: 0021-9991. doi: https://doi.org/10.1016/j.jcp.2022.111041. Disponível em: <https://www.sciencedirect.com/science/article/pii/S0021999122001036>.

MEHMANI, Y., XU, K., 2022b, "Pore-network modeling of Ostwald ripening in porous media: How do trapped bubbles equilibrate?" *Journal of Computational Physics*, v. 457, pp. 111041. ISSN: 0021-9991. doi: https://doi.org/10.1016/j.jcp.2022.111041. Disponível em: <https://www.sciencedirect.com/science/article/pii/S0021999122001036>.

MEHMANI, Y., OOSTROM, M., BALHOFF, M. T., 2014, "A streamline splitting pore-network approach for computationally inexpensive and accurate simulation of transport in porous media", *Water Resources Research*, v. 50, n. 3, pp. 2488–2517.

O'NEILL, M. E., 2014, "PCG: A family of simple fast space-efficient statistically good algorithms for random number generation", *ACM Transactions on Mathematical Software*.

PLAUTZ, D. A., JOHNSTONE, H. F., 1955, "Heat and mass transfer in packed beds", *AIChE Journal*, v. 1, n. 2, pp. 193–199.

ROBBINS, G. A., 1989, "Methods for determining transverse dispersion coefficients of porous media in laboratory column experiments", *Water Resources Research*, v. 25, n. 6, pp. 1249–1258.

ROEMER, G., DRANOFF, J. S., SMITH, J. M., 1962, "Diffusion in packed beds at low flow rates", *Industrial and Engineering Chemistry Fundamentals*, v. 1, n. 4, pp. 284–287.

SAFFMAN, P. G., 1959, "Dispersion in flow through a network of capillaries", *Chemical Engineering Science*, v. 11, n. 2, pp. 125–129.

SAHIMI, M., 2011, *Flow and transport in porous media and fractured rock: from classical methods to modern approaches*. USA, South California, John Wiley and Sons.

SALLES, J., THOVERT, J. F., DELANNAY, R., et al., 1993, "Taylor dispersion in porous media. Determination of the dispersion tensor", *Physics of Fluids A: Fluid Dynamics*, v. 5, n. 10, pp. 2348–2376.

SCHEIDEGGER, A. E., 1957, *The physics of flow through porous media*. Canada, Toronto, University of Toronto press.

SCHENK, O., GÄRTNER, K., FICHTNER, W., et al., 2001, "PARDISO: a high-performance serial and parallel sparse linear solver in semiconductor device simulation", *Future Generation Computer Systems*, v. 18, n. 1, pp. 69–78. ISSN: 0167-739X. doi: https://doi.org/10.1016/S0167-739X(00)00076-5. Disponível em: <https://www.sciencedirect.com/science/article/pii/S0167739X00000765>. I. High Performance Numerical Methods and Applications. II. Performance Data Mining: Automated Diagnosis, Adaption, and Optimization.

SINCLAIR, R. J., POTTER, O. E., 1965, "Dispersion of gas in flow through a bed of packed solids", *TRANSACTIONS OF THE INSTITUTION OF CHEMICAL ENGINEERS AND THE CHEMICAL ENGINEER*, v. 43, n. 1, pp. T3.

SLATTERY, J. C., 1972, "Momentum, energy, and mass transfer in continua", *(No Title)*.

SLICHTER, C., 1905, "Field measurements of the rate of movement of underground waters", *US Gelogical Survey Water-Supply and Irrigation Paper*, v. 140.

SUN, N., SUN, A., 2014, *Mathematical Modeling of Groundwater Pollution*. China, Springer New York. ISBN: 9781475725582. Disponível em: <https://books.google.co.uk/books?id=tykBCAAAQBAJ>.

TARTAKOVSKY, A. M., MEAKIN, P., SCHEIBE, T. D., et al., 2007, "A smoothed particle hydrodynamics model for reactive transport and mineral precipitation in porous and fractured porous media", *Water resources research*, v. 43, n. 5.

TAYLOR, G. I., 1953, "Dispersion of soluble matter in solvent flowing slowly through a tube", *Proceedings of the Royal Society of London. Series A. Mathematical and Physical Sciences*, v. 219, n. 1137, pp. 186–203.

TOWLE, W. L., SHERWOOD, T. K., 1939, "Studies in eddy diffusion", *Ind Eng Chem*, v. 31, n. 1, pp. 457.

VAN GENUCHTEN, M. T., 1982, *Analytical solutions of the one-dimensional convective-dispersive solute transport equation*. USA, US Department of Agriculture, Agricultural Research Service.

VAN GORP, R., VAN DER HEIJDEN, M., AMIN SADEGHI, M., et al., 2023, "Bottom-up design of porous electrodes by combining a genetic algorithm and a pore network model", *Chemical Engineering Journal*, v. 455, pp. 139947. ISSN: 1385-8947. doi: https://doi.org/10.1016/j.cej.2022.139947. Disponível em: <https://www.sciencedirect.com/science/article/pii/S1385894722054274>.

VIRTANEN, P., GOMMERS, R., OLIPHANT, T. E., et al., 2020, "SciPy 1.0: fundamental algorithms for scientific computing in Python", *Nature methods*, v. 17, n. 3, pp. 261–272.

WEISHAUPT, K., JOEKAR-NIASAR, V., HELMIG, R., 2019, "An efficient coupling of free flow and porous media flow using the pore-network modeling approach", *Journal of Computational Physics: X*, v. 1, pp. 100011.

WHITAKER, S., 1999, *The Method of Volume Averaging*. USA, California, Springer Science+Business Media Dordrecht.

WHITAKER, S., 1967, "Diffusion and dispersion in porous media", *AIChE Journal*, v. 13, n. 3, pp. 420–427.

XIE, C., LEI, W., BALHOFF, M. T., et al., 2021, "Self-adaptive preferential flow control using displacing fluid with dispersed polymers in heterogeneous porous media", *Journal of Fluid Mechanics*, v. 906, pp. A10.

YANG, X., MEHMANI, Y., PERKINS, W. A., et al., 2016, "Intercomparison of 3D pore-scale flow and solute transport simulation methods", *Advances in Water Resources*, v. 95, pp. 176–189. ISSN: 0309-1708. doi: https://doi.org/10.1016/j.advwatres.2015.09.015. Disponível em: <https://www.sciencedirect.com/science/article/pii/S0309170815002225>. Pore scale modeling and experiments.

Appendix A

Analytical Solutions

A.1 Separation of variables

Once the dimensionless concentration, $\bar{\phi}$, depends on the dimensionless axial, ζ, and radial direction, η, we can write $\phi(\zeta,\eta) = X(\zeta)Y(\eta)$, and substitute it into Equation 3.3 to obtain:

$$\frac{Pe_B X_R' X''}{X} = \frac{Y''}{Y} = -\lambda^2 \tag{A.1}$$

where λ is the eigenvalue of this problem. The following system and its boundary condition, Equation A.3, is generated and can be written as

$$Y_n'' + \lambda_n^2 Y_n = 0 \tag{A.2}$$

$$Y_n'(0) = 0 \qquad Y_n(1) = 0 \tag{A.3}$$

with its solution being

$$Y_n(\eta) = A_n cos(\lambda_n \eta) + B_n sen(\lambda_n \eta) \tag{A.4}$$

So, $Y_n'(\eta) = \lambda_n \left[-A_n sen(\lambda_n \eta) + B_n cos(\lambda_n \eta)\right]$ and when the boundaries conditions are applied, the values of these constants are obtained as $B_n = 0$ and $\lambda_n = \pi\left(n + \frac{1}{2}\right)$, where $n = 0, 1, 2, ...$

A.2 Semi-infinite domain

For $X(\zeta)$, the ODE is represented below.

$$RX'' - Pe_B X' - \lambda_n^2 X = 0 \tag{A.5}$$

This equation has the form of $Rr^2 - Pe_B r - \lambda_n^2 = 0$, where the roots have the following form:

$$r = \frac{Pe_B \pm [Pe_B^2 + 4R\lambda_n^2]^{1/2}}{2R} = \frac{Pe_B}{2R}\left[1 \pm \left(1 + \frac{4R\lambda_n^2}{Pe_B^2}\right)^{1/2}\right]$$

Considering r_1 and r_2 the distinct roots of the indexing equation with $r_1 > r_2$, the signal $\pm$ will be positive or negative when the interested root is r_1 or r_2, respectively. Note that for each λ_n, we have new roots. The solution for this ODE is given as:

$$X_n(\zeta) = h_n \exp(r_{1n}\zeta) + p_n \exp(r_{2n}\zeta) \tag{A.6}$$

Note that the infinite boundary condition ($\zeta \to \infty, \quad \phi = 0$) is satisfied only when the negative root remains, in other words, that means $h_n = 0$. The final form of $X_n(\zeta)$ is:

$$X_n(\zeta) = p_n \exp\left(\frac{Pe_B}{2R}\zeta\left[1 - \left(1 + \frac{4\lambda_n^2 R}{Pe_B^2}\right)^{1/2}\right]\right) \tag{A.7}$$

It is worthy to highlight that $\frac{Pe_B}{R} = \frac{Pe_L}{A} = \frac{uB}{D_L}$ and hence Equation A.7 has a dependence on both dispersion coefficients.

The analytical solution is presented as Equation A.8, where the exponential term is a function of ζ and is defined as $f(\eta)$.

$$\phi(\zeta,\eta) = \sum_{n=0}^{\infty} C_n cos(\lambda_n \eta) \underbrace{\exp\left(\frac{Pe_B}{2R}\zeta\left[1 - \left(1 + \frac{4R\lambda_n^2}{Pe_B^2}\right)^{1/2}\right]\right)}_{g(\eta)} \tag{A.8}$$

When the boundary condition $\phi(0,\eta) = 1$ is used, the value of the C_n can be determined as

$$C_n = \frac{\int_0^1 cos(\lambda_n \eta) d\eta}{\int_0^1 cos^2(\lambda_n \eta) d\eta} = \frac{4sen(\lambda_n)}{2\lambda_n + sen(2\lambda_n)} \tag{A.9}$$

Once C_n is obtained, Equation A.8 can be integrated in the cross-section area normal to the flow direction, defining the mean dimensionless concentration given by Equation A.10

$$\bar{\phi}(\zeta) = \sum_{n=0}^{\infty} C_n \left(\int_0^1 cos(\lambda_n \eta) d\eta \right) f(\zeta) \tag{A.10}$$

where $\int_0^1 cos(\lambda_n \eta) d\eta = \frac{sen(\lambda_n)}{\lambda_n}$.

At the end, with all the terms written and replaced the final equation for infinite domain is

$$\bar{\phi}(\zeta) = \sum_{n=0}^{\infty} \frac{2}{\lambda_n^2} \exp \left\{ \frac{Pe_B}{2R} \zeta \left[1 - \left(1 + \frac{4R\lambda_n^2}{Pe_B^2} \right)^{1/2} \right] \right\} \tag{A.11}$$

A.3 Finite domain

For the case where a limited length is imposed to the domain, the boundary condition used is ($\zeta = A$, $\frac{\partial \phi}{\partial \zeta} = 0$) in Equation A.6, resulting in:

$$h_n r_{1n} \exp(r_{1n} A) = -p_n r_{2n} \exp(r_{2n} A) \tag{A.12}$$

It is important to recall that the roots are the same found for the infinite boundary condition, and as $r_{1n} > 0$ and $A > 1$, the exponential term $\exp(r_{1n} A)$ increases rapidly with n. Because of that, it is better to write this term as a denominator to avoid numerical issues as shown below:

$$h_n = -pn \frac{r_{2n} \exp(r_{2n} A)}{r_{1n} \exp(r_{1n} A)} \tag{A.13}$$

Replacing h_n in Equation A.12, one can find:

$$X_n(\zeta) = p_n \left[-\frac{r_{2n}}{r_{1n}} \exp(r_{2n} A) \exp(-r_{1n}(A - \zeta)) + \exp(r_{2n} \zeta) \right] \tag{A.14}$$

As $|r_{1n}| > |r_{2n}|$ and $r_{2n} < 0$, $r_{1n} > 0$, it is concluded that $0 < \exp(r_{2n} A) < 1$ and

that the following inequality is valid as shown below:

$$0 < \frac{-r_{2n}}{r_{1n}} < 1 \quad \rightarrow \quad 0 < \frac{-r_{2n}}{r_{1n}} \exp(r_{2n}A) < 1 \tag{A.15}$$

Also, as Pe_B, R, A and λ_n define this value, we can say that the above expression can be replaced by q_n, in other words we can write

$$q_n = \frac{-r_{2n}}{r_{1n}} \exp(r_{2n}A), 0 < q_n < 1 \tag{A.16}$$

and the $X_n(\zeta)$ solution can be written as

$$X_n(\zeta) = p_n g_n(\zeta) \tag{A.17}$$

where $g_n(\zeta) = \exp(r_{2n}\zeta) + q_n \exp(-r_{1n}(A-\zeta))$. So the series solution takes the form of

$$\phi(\zeta, \eta) = \sum_{n=0}^{\infty} \bar{C_n} cos(\lambda_n \eta) g_n(\zeta) \tag{A.18}$$

Using the non-homogeneous boundary condition, $\phi = 1$, $\zeta = 0$, it is possible to obtain the constant $\bar{C_n}$ value as shown below.

$$\phi(0, \eta) = \sum_{n=0}^{\infty} \bar{C_n} cos(\lambda_n \eta) g_n(0) \tag{A.19}$$

Note that $g_n(0) = 1 + q_n \exp(-r_{1n}A)$ and using the orthogonality properties, we can find that:

$$\bar{C_n} g_n(0) = \frac{\int_0^1 cos(\lambda_n \eta) d\eta}{\int_0^1 cos^2(\lambda_n \eta) d\eta} = \frac{4sen(\lambda_n)}{2\lambda_n + sen(2\lambda_n)} = C_n \tag{A.20}$$

$$\bar{C_n} = \frac{C_n}{g_n(0)} \tag{A.21}$$

On this way it is concluded that $\phi(\eta, \zeta)$ can be written as Equation A.22, where in analogies with what was done for the infinite domain, this equation was inte-

grated into the cross-section area of the domain to find the mean dimensionless concentration as described by Equation A.23.

$$\phi(\zeta,\eta) = \sum_{n=0}^{\infty} C_n cos(\lambda_n \eta) \frac{g_n(\zeta)}{g_n(0)} \tag{A.22}$$

$$\bar{\phi}(\zeta) = \sum_{n=0}^{\infty} C_n \left[\int_0^1 cos(\lambda_n \eta) d\eta\right] \frac{g_n(\zeta)}{g_n(0)} \tag{A.23}$$

Replacing C_n and the value of the integral in Equation A.23, the final solution for the mean dimensionless concentration is found as:

$$\bar{\phi}(\zeta) = \sum_{n=0}^{\infty} \frac{2}{\lambda_n^2} \left[\frac{\exp(r_{2n}\zeta) - \left(\frac{r_{2n}}{r_{1n}}\right) \exp\left[A(r_{2n} - r_{1n}) + r_{1n}\zeta\right]}{1 - \left(\frac{r_{2n}}{r_{1n}}\right) \exp[(r_{2n} - r_{1n})A]}\right] \tag{A.24}$$